AD-A146 557 INTERFACE STRUCTURES FOR MILLIMETER-WAVE CIRCUITS(U) 1/1
TEXAS UNIV AT AUSTIN DEPT OF ELECTRICAL AND COMPUTER
ENGINEERING T ITOH 25 SEP 84 ARO-17735.36-EL
UNCLASSIFIED DAAG29-81-K-0053 F/G 9/5 NL

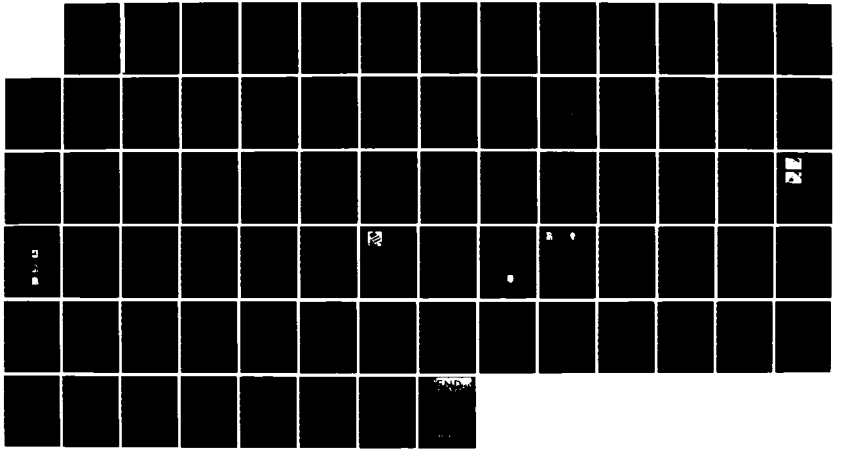

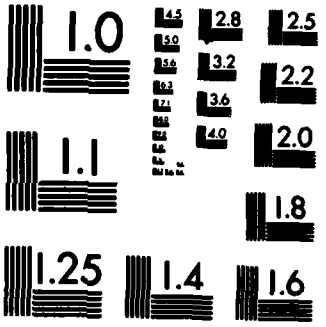

(2)

Interface Structures for Millimeter-Wave Circuits

Final Report

by

Tatsuo Itoh

September 25, 1984

U.S. Army Research Office

Contract No.: DAAG29-81-K-0053

The University of Texas at Austin
Department of Electrical and Computer Engineering
Austin, Texas 78712

UNCLASSIFIED
SECURITY CLASSIFICATION OF THIS PAGE (When Data Entered)

MASTER COPY - FOR REPRODUCTION PURPOSES

REPORT DOCUMENTATION PAGE

READ INSTRUCTIONS BEFORE COMPLETING FORM

1. REPORT NUMBER	2. GOVT ACCESSION NO. AD-A146557 ~~N/A~~
3. RECIPIENT'S CATALOG NUMBER N/A	
4. TITLE (and Subtitle) Interface Structures for Millimeter-Wave Circuits	5. TYPE OF REPORT & PERIOD COVERED Final Report March 1, 1981-August 31, 1984
	6. PERFORMING ORG. REPORT NUMBER
7. AUTHOR(s) Tatsuo Itoh	8. CONTRACT OR GRANT NUMBER(s) DAAG29-81-K-0053
9. PERFORMING ORGANIZATION NAME AND ADDRESS Department of Electrical & Computer Engineering University of Texas Austin, Texas 78712	10. PROGRAM ELEMENT, PROJECT, TASK AREA & WORK UNIT NUMBERS
11. CONTROLLING OFFICE NAME AND ADDRESS U. S. Army Research Office Post Office Box 12211 Research Triangle Park, NC 27709	12. REPORT DATE September 25, 1984
	13. NUMBER OF PAGES 70 pages incl. Appendices
14. MONITORING AGENCY NAME & ADDRESS (if different from Controlling Office)	15. SECURITY CLASS. (of this report) Unclassified
	15a. DECLASSIFICATION/DOWNGRADING SCHEDULE

16. DISTRIBUTION STATEMENT (of this Report)

Approved for public release; distribution unlimited.

17. DISTRIBUTION STATEMENT (of the abstract entered in Block 20, if different from Report)

NA

18. SUPPLEMENTARY NOTES

The view, opinions, and/or findings contained in this report are those of the author(s) and should not be construed as an official Department of the Army position, policy, or decision, unless so designated by other documentation.

19. KEY WORDS (Continue on reverse side if necessary and identify by block number)

Dielectric waveguides, quasi-optical structures, printed transmission lines, Gain devices, slow-wave structures

20. ABSTRACT (Continue on reverse side if necessary and identify by block number)

This report summarizes research activities at the Microwave Laboratory, University of Texas on various structures for millimeter-wave circuits under sponsorship of the U.S. Army Research Office Contract DAAG29-81-K-0053. The topics of investigation include quasi-optical mixers, E-plane filters, printed transmission lines, distributed gain mechanisms, slow-wave phenomena and dielectric waveguides. A list of publications is included.

DD FORM 1 JAN 73 1473 EDITION OF 1 NOV 65 IS OBSOLETE

UNCLASSIFIED
SECURITY CLASSIFICATION OF THIS PAGE (When Data Entered)

Interface Structures for Millimeter-Wave Circuits

Final Report

by

Tatsuo Itoh

September 25, 1984

U.S. Army Research Office

Contract No.: DAAG29-81-K-0053

The University of Texas at Austin
Department of Electrical and Computer Engineering
Austin, Texas 78712

**APPROVED FOR PUBLIC RELEASE:
DISTRIBUTION UNLIMITED**

TABLE OF CONTENTS

LIST OF APPENDICES

Abstract

This report summarizes research activities at the Microwave Laboratory, University of Texas on various structures for millimeter-wave circuits under sponsorship of the U.S. Army Research Office Contract DAAG29-81-K-0053. The topics of investigation include quasi-optical mixers, E-plane filters, printed transmission lines, distributed gain mechanisms, slow-wave phenomena and dielectric waveguides. A list of publications is included.

1. Introduction

During the past several years, millimeter-wave techniques especially in the form of printed circuits[1,2] and dielectric waveguide [3,4] have been developed at a rapid pace. Many high performance components and devices have been produced and tested as exemplified in a recent Special Issue on Millimeter Waves of IEEE Transactions on Microwave Theory and Techniques[5]. In addition, studies on fundamental characteristics of guided waves in various transmission media have been performed and the concept of open structures has been applied to investigate systematically the dielectric waveguides and printed transmission lines [6,7,8]. With the advent of monolithic integrated circuits, it becomes more important to consider the guided waves in various configurations containing not only the passive but also active and nonlinear materials. As quasi-optical structures are important at extremely high millimeter-wave frequencies, the radiating nature of the guided wave structures must also be studied.

Over the past three years, a number of projects on the interfacing between the active and passive structures and the waves in semiconductor materials have been studied at the University of Texas under the support of DAAG29-81-K-0053 from the Army Research Office. This report summarizes all of these projects and the publications resulting therefrom.

2. Dielectric Waveguides

Although understanding of the guided wave natures of dielectric waveguides for millimeter-wave integrated circuits has reached a certain maturity, there still remains fundamental difficulty in the

use of them for practical circuits. Due to their open nature, these waveguides easily radiate at discontinuities, bends and interfaces with active device[9]. A number of projects have been undertaken that provide more useful configurations and a mechanism to interface with printed transmission lines.

2.1 Accurate analysis of a trapped image guide

The trapped image guide consists of a rectangular dielectric rod placed in a metal trough so that the radiation loss at a sideward bend and an undesirable coupling to other parts of the circuits can be reduced.[10]. Instead of the conventional effective dielectric constant approach, an improved analysis method has been developed. In this technique, the field inside the trough is analyzed by the effective dielectric constant method but the field outside the trough is expanded in terms of Weber-Schafheitlin integrals which automatically satisfy the electric boundary conditions on the ground plane. A mode matching technique is implemented at the interface between the trough interior and the external free space. Experimental data for Ku-band agreed with the theoretical results.[11].

2.2 Hollow image guide

The hollow image is a modification of an image guide, consisting of a rectangular dielectric rod with a hollow core placed on a ground plane (Fig. 1). This core can be filled with another material, if necessary. The propagation characteristic of the guide can be controlled with the size of the core, thereby increasing the degree of fredom in design. The core can be used to house an active device or

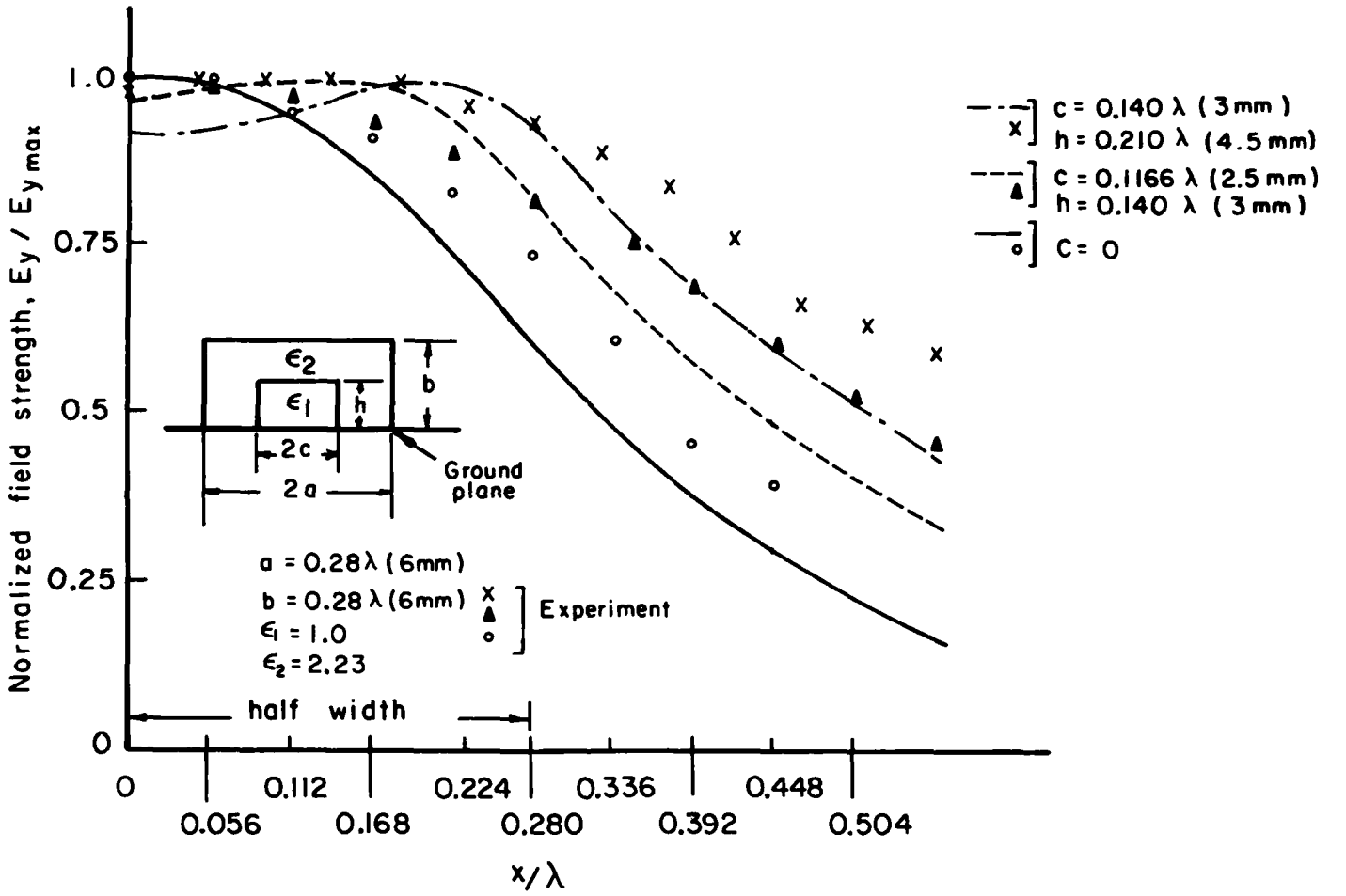

FIGURE 1 - Hollow Image Guide

to provide a tapered transition. An analysis based on the effective dielectric constant method has been developed and the numerical results compared with experimental data.

The hollow image guide can also be thought of as a directional coupler consisting of two image guides with a dielectric overlay. The degree of coupling can be adjusted by the thickness of the overlay (or by size of the hollow core). The coupling characteristics have been studied both theoretically and experimentally. The experimental study was conducted by design, fabrication and test of a 3-dB directional coupler. Excellent agreement has been obtained between theory and experiment[12].

2.3 Coupling between an image guide and a printed transmission line

Direct implementation of solid state devices in a dielectric waveguide is undesirable for two reasons. First, any discontinuities generated by implementation of active devices cause radiation from the dielectric waveguide[9]. Second, the most presently available devices are designed to be implemented either in a metal waveguide or in a printed transmission line. Therefore, a good transition between the dielectric waveguide and the printed transmission line is useful. If such is available, the device can be placed in a printed line environment with good control of characteristics.

Fig. 2 shows a transition from an image guide to a microstrip line via a number of slots in a common ground plane[13]. A method based on a perturbation approach has been used for analysis and design of the structure. In this approach, equivalent electric and magnetic dipole moments of the slot are obtained from the modal field in the

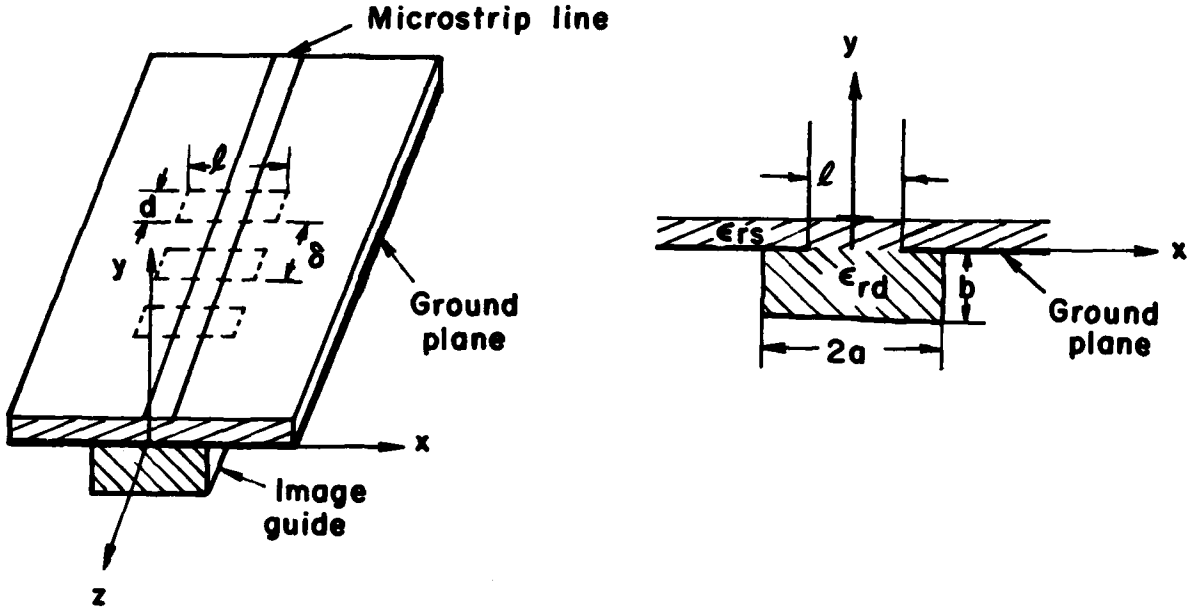

FIGURE 2 - Coupling between an image guide and a microstrip line

microstrip line. The latter is calculated by introduction of an equivalent waveguide model of the microstrip line. From these electric and magnetic dipoles, the amplitude of the fundamental mode E^y_{11} excited in the image guide is calculated.

Once this information is available, a directive coupling structure can be designed. A 15-dB five-slot Chebyshev coupler has been designed for X-band. Theoretical and experimental results for the coupling agree well and are essentially flat over the frequency range of 8.5 to 10.5 GHz. The reverse coupling is better than -30 dB though the theory predicted -40 dB.

3. Quasi-Optical Structures

At extremely high frequencies, quasi-optical structures are useful as they have minimal insertion loss between the free space to the RF front end. Recently, a monolithically oriented configuration has been introduced especially in the area of mixers[14]. Essentially, the RF input is capture by a printed antenna which is a port of the mixer circuits. LO signals are fed either via a waveguide or a printed line and an IF is extracted by a printed line. We have created, analyzed, designed and tested two entirely different quasi-optical mixers, both of which are extremely well suited for monolithic integration at millimeter-wave frequencies. One of them can also be used as a frequency multiplier with a double sideband suppressed carrier.

3.1 Polarization duplexed planar balanced mixer

Fig. 3 shows the polarization duplexed balanced mixer. It is

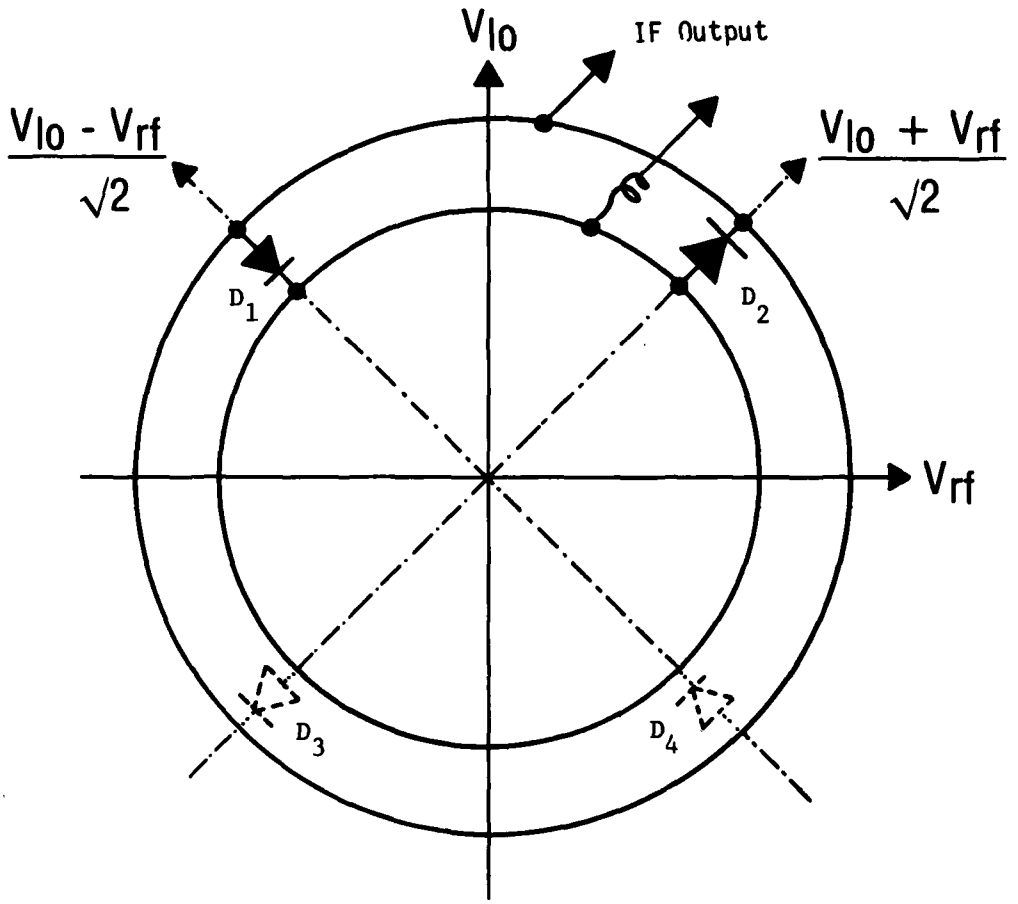

FIGURE 3 - Schematic of a polarization duplexed balanced mixer

made of a slot line ring resonator which also acts as a printed antenna. Two mixer diodes are placed at 90 degrees apart as shown. When this structure is illuminated with RF and LO plane wave signals with orthogonal polarizations, a phasing is applied to each diode that is appropriate for balanced mixer operation.

First, the characteristics of appropriate sized ring antennas have been calculated and measured up to 95 GHz. The mixer experiments have been conducted at X band and a conversion loss as good as 6.5 dB has been obtained. Due to orthogonally polarized RF and LO, their isolation is better than 30 dB and the cross-polarization rejection is 20 dB[15]. The University of Texas System is filing a U.S. patent on this invention.

3.2 Planar quasi-optical subharmonic mixer

It is known that a bowtie antenna has a broad operating bandwidth as demonstrated in use for a UHF television reception. This antenna is, therefore, ideally suited for a quasi-optical subharmonically pumped mixer in which the local oscillator signal with one half the RF signal frequency is used. In the proposed scheme, two antiparallel mixer diodes are mounted between the two electrodes of the bowtie antenna. The RF and LO signals with identical polarizations illuminate the antenna and mixed-down IF signals are extracted by a printed line or a coaxial from the ends of the bowtie. A simple theory has been developed for the antenna characteristics and its accuracy has been confirmed experimentally. For 14 GHz RF input, the conversion loss was 8.6 dB and the same structure actually responded for operation beyond 35 GHz. A properly scaled version is hence

expected to perform well at much higher frequencies.

3.3 Frequency doubler

By using the subharmonically-pumped bowtie mixer described above in a backward sense, the identical structure may be used as a frequency doubler with a double sideband suppressed carrier. The bowtie antenna loaded with two antiparallel mixer diodes is illuminated by an LO signal. When an IF signal is injected, the structure radiates a second harmonic signal. An efficiency of 1~ 3% has been observed for a 14 GHz output[17].

4. Printed Transmission Line Structure

For millimeter-wave circuits with the signal frequency up to at least 140 GHz, printed transmission lines are used in the majority of configurations. It is necessary, however, that a good choice of configuration must be made for a particular application. Printed transmission lines other than the microstrip line are often more desirable at higher frequencies. Finlines or E-plane circuits and suspended striplines are two of the examples preferred at millimeter-wave frequencies. E-plane filters, suspended patch antennas and finline discontinuities have been studied in the past three years.

4.1 E-plane filters

Several representative E-plane filter configurations are shown in Fig. 4. These structures have been analyzed based on the residue calculus technique[18] and the generalized scattering matrix method[19] All of the structures in Fig. 4 can be handled by these techniques.

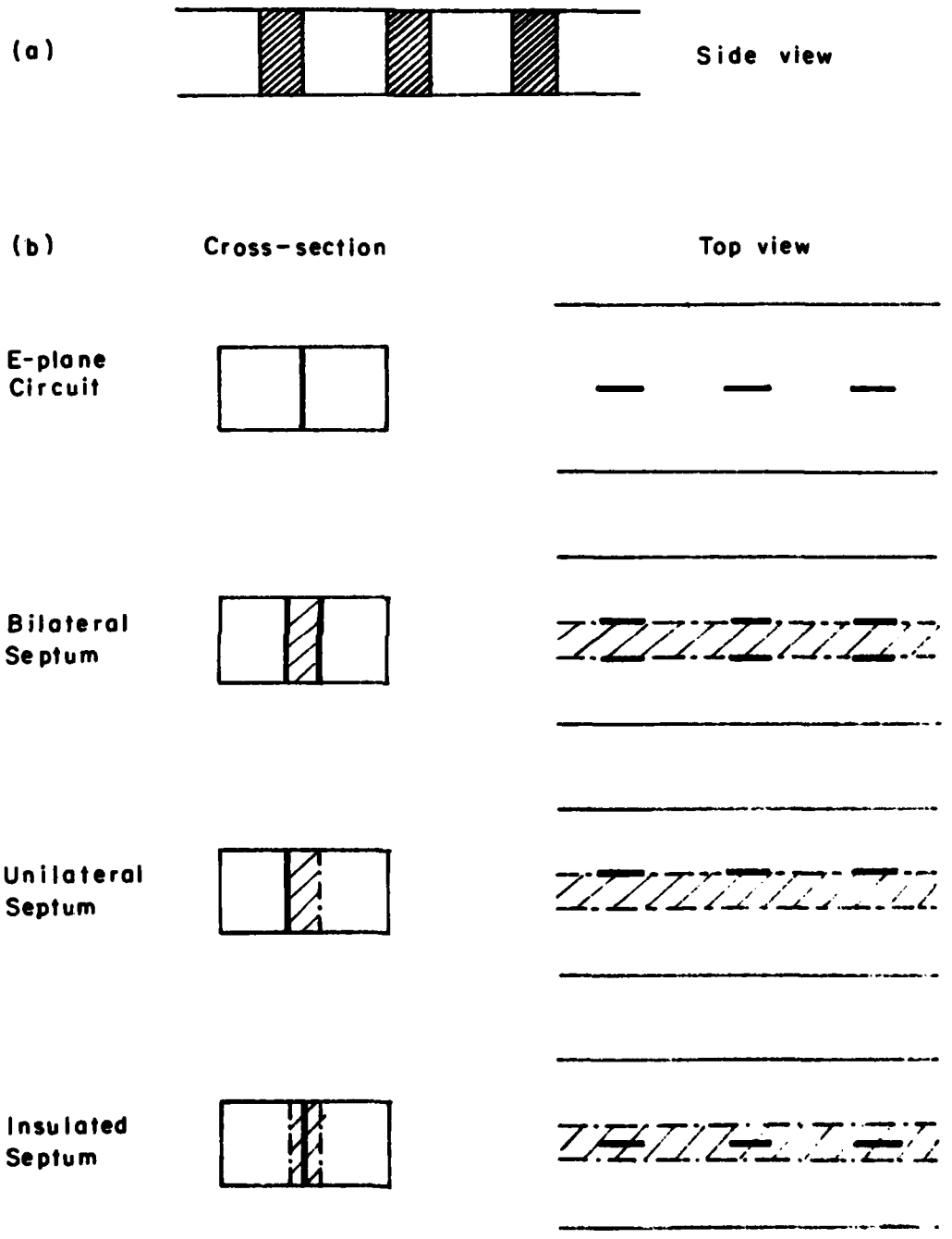

FIGURE 4 - E-plane filters

First, the scattering characteristics of the edge of a fin are obtained in a closed form from the residue calculus technique. Next, the generalized scattering matrix technique is used to combine the scattering phenomena at two edges. This process results in the generalized S matrix of the fin. Notice that interactions not only by the dominant mode but by all the higher order modes are included. Hence, the results are very accurate even for an extremely narrow fin. Next, the generalized S matrix of the first fin is connected to that of the second fin by way of a generalized transmission matrix containing all the modes. This process is repeated until the last fin is included. The result is the generalized S matrix of the filter structure.

When a filter is designed, a computer optimization can be used in which all the structural parameters are systematically adjusted until the desired transfer characteristics result[20]. Another approach based on a filter synthesis technique has recently been proposed[21]. In this approach a low-pass prototype filter has been used as a starting point of synthesis[22], and a substantial saving in computation time has been attained.

4.2 Electromagnetically coupled patch antenna

One way to increase the performance of a patch antenna is to elevate the patch from the ground plane. A structure studied in this project is to place a rectangular patch on a substrate which is in turn elevated from the ground plane. An inverted microstrip placed underside of the substrate can excite this patch antenna by way of electromagnetic coupling.

The first attempt at this problem treated a special case where the inverted strip feed terminated exactly below the edge of the suspended patch and hence no overlapping section existed[23]. The spectral domain method was used to characterize the inverted and suspended line. From the results, the former is replaced with an equivalent waveguide and the latter with an equivalent resonator both of which have magnetic side walls. Next, a simple theory based on the reaction concept was applied to excitation of the hypothetical equivalent cavity by a hypothetical equivalent waveguide. The calculated input impedance agreed well with experimental data.

The second analysis was done on the basis of transmission line model and microwave network theory[24]. We recognize that the patch is an open-ended suspended strip resonator. The structure is divided into three parts. Region I is the inverted microstrip line, Region II is the overlapping section of the suspended line and an inverted line, and Region IV is th open-ended suspended line. In the analysis, the 4-port impedance matrix of Region II is calculated. Note that even and odd modes do not exist in this region because the coupled lines are nonsymmetric and inhomogeneous. Next the open ends of the suspended patch are modeled with termination by quasi-static capacitances and radiation conductances. The input impedance of the system seen from the inverted microstrip in Region I can now be calculated. The numerical results agreed well with the experimental data and indicate that there are two optimum coupling lengths for this particular set of structural parameters.

4.3 Overlay directional coupler

It has been known that a microstrip directional coupler can be made broadband by placing an overlay (superstrate). Surprisingly, however, no full-wave analysis has existed. In this project, a general layered printed coupled line has been analyzed with the spectral domain method. A 10-dB overlay coupler was built according to the design theory and the experimental results agreed well with theoretical prediction[25].

4.4 Finline discontinuity

Although a fair amount of information is now available for microstrip discontinuities, the situation is not true for other millimeter-wave printed transmission lines[26]. This project deals with a step discontinuity in a finline. The first step is to create a resonator by inserting short-circuited walls at distances sufficiently away from the discontinuity. The transverse resonance technique is used to derive a resonant frequency. We find three different resonator sizes that give rise to the same resonant frequency. From these lengths, the equivalent T or π network of the discontinuity is evaluated. The results were compared with other available data[27]. This project will be carried over to the next period under a new contract and cascaded discontinuities will be studied.

4.5 VLSI interconnect line

As the speed of digital circuit increases, the electromagnetic nature of the pulse transmission will eventually appear. For instance, at clock rates of 10 Gbits/sec, the clock harmonics are well into the millimeter-wave range (30-300 GHz). In such a situation,

traditional analyses for interconnect lines by distributed RC network[28] and a quasi-static capacitance matrix[29] encounter limitations. The full-wave analysis based on the spectral domain approach has been applied to a coupled pair of strips located at different interfaces[30]. This method is capable of predicting frequency dispersion of the line parameters and is useful for investigation of coupling between adjacent lines and the input and output impedances.

5. Gain devices

A good solid state source is one of the most critical elements for millimeter-wave integrated circuits, especially the one suitable for monolithic integration. A distributed solid state source provides an alternative to traditional lumped element devices. There are a number of advantages. The deteriorated characteristics at higher frequencies can be compensated for by accumulative effects. Distributed inductance and capacitance may be embedded in a transmission line typically formed by electrodes. Although these devices have been conceived for a number of years, difficulty in fabrication was not resolved until recently. With the advent of MBE and other processing techniques such a "large" device can now be fabricated.

Initially, we studied theoretically and experimentally a distributed Gunn diode. In the device fabricated according to the theory developed, the existence of the gain was confirmed. However, the series resistance in the ohmic contacted electrode was too great to result in the device gain.

Recently, Texas Instruments was successful in fabricating distribute IMPATT diodes[31]. This structure (Fig. 5) has been analyzed by means of Runge-Kutta techniques to solve coupled differential equations describing the distributed IMPATT operation under a small signal assumption. The results successfully explained the experimental characteristics of the device[32].

Another approach for a high frequency source can be a transmission line periodically loaded with IMPATT diodes. The diode and the mounting structure have been first characterized as an impedance post. The active impedance associated with the diode has been obtained by means of a Runge-Kutta approach. The entire structure has been analyzed by successive impedance transformation. A resonant characteristic dictated by the period has been obtained. The results need to be confirmed by experimental verification.

With increased frequency cutoff of an FET, it is important to characterize the device behavior accurately. An attempt has been initiated to simulate the FET characteristics based on the finite element analysis. This effort will be carried forward.

6. Slow-wave structures

Recently, the slow-wave phenomena have drawn considerable attention in connection with monolithic microwave integrated circuits[33]. Both MIS and Schottky contact microstrip and coplanar structures have been analyzed under this program using the spectral domain method. The slow-wave phenomena are caused by the loss mechanism in the substrate. The slow-wave phenomena gradually deteriorate and the attenuation increases as the frequency is

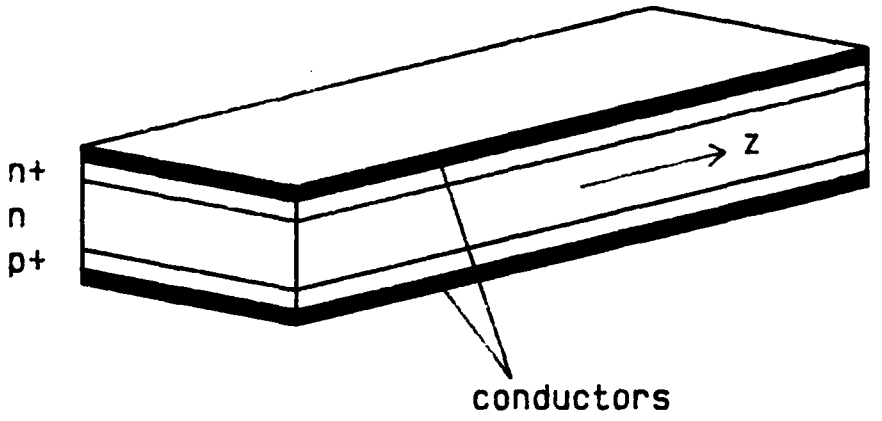

Figure 5. Single-drift distributed IMPATT diode

increased. Use of periodic structures (Fig. 6) has been conceived for extending the frequency range. It was found that the loss is smaller and that the slow-wave phenomena is enhanced with an appropriate choice of parameters.

Based on these analyses, a distributed electronic phase shifter is proposed and analyzed. The present result shows that a 180 degree phase shifter with a reasonable insertion loss may be possible in the millimeter wave region[34].

7. Conclusions

In this report, we summarized the projects carried out under sponsorship of DAAG29-81-K-0053. Some problems included in this report require further investigation during the next contract period.

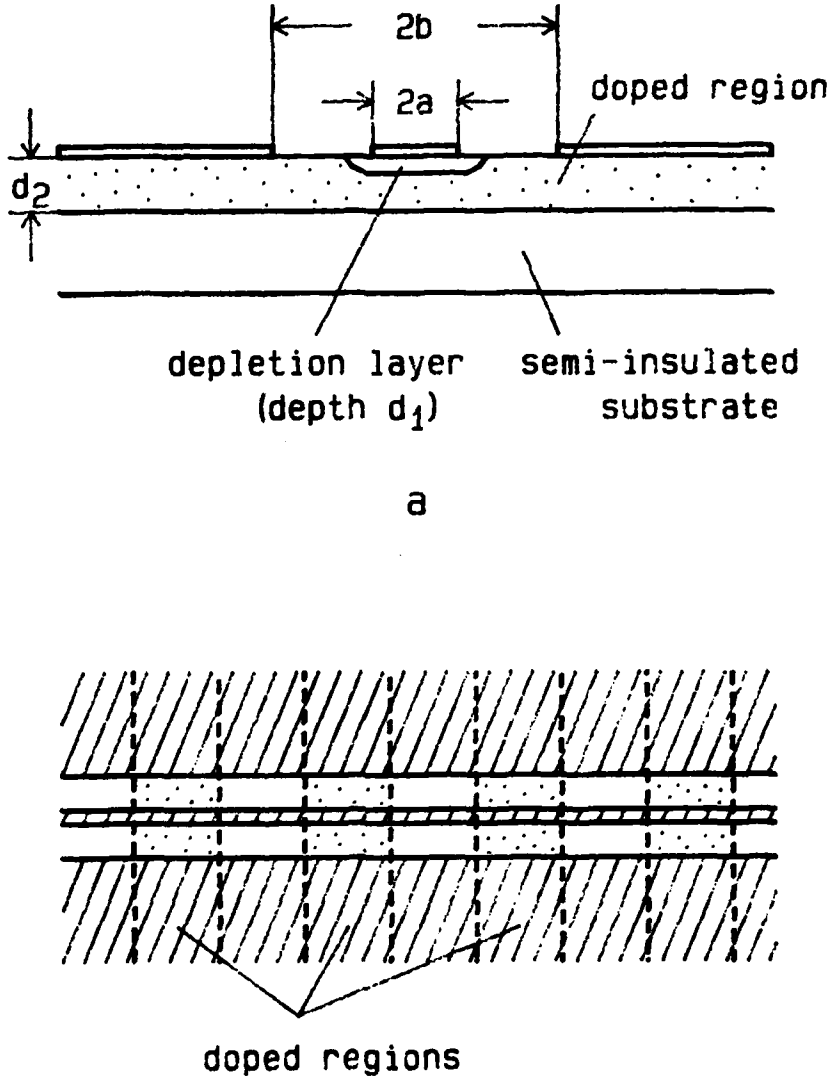

Figure 6 - Periodically doped Schottky contact coplanar waveguide

(a) Cross Section

(b) Top View

REFERENCES

1. E. R. Carlson, M.V. Schneider, and T.F. McMaster, "Subharmonically pumped millimeter-wave mixers," IEEE Trans. Microwave Theory and Tech., Vol. MTT-26, pp. 706-715, October 1978.

2. L. Bui and D. Ball, "Broadband planar balanced mixers for millimeter-wave applications," 1982 IEEE MTT-S International Microwave Symposium, Dallas, Texas, pp. 204-205, June 1982.

3. H. Jacobs, G. Novick, C.M. LoCoscio and M.M. Chrepta, "Measurement of guided wavelength in rectangular dielectric waveguide," IEEE Trans. Microwave Theory and Tech., Vol. MTT-24, pp. 815-820, November 1976.

4. R.M. Knox, "Dielectric waveguide microwave integrated circuits - an overview," IEEE Trans. Microwave Theory and Tech., Vol. MTT-24, pp. 806-814, November 1976.

5. V.G. Glenovatch and H. Jacobs (ed.) Special Issue on Millimeter-waves, IEEE Trans. Microwave Theory and Tech., Vol. MTT-31, February 1983.

6. D.C. Chang, "Analytical theory of an unloaded rectangular microstrip patch," IEEE Trans. Antennas and Propagation, Vol. AP-29, pp. 54-62, January 1981.

7. S.T. Peng and A.A. Oliner, "Guidance and leakage properties of a class of open dielectric waveguides: Part I - Mathematical formulations," IEEE Trans. Microwave Theory and Tech., Vol. MTT-29, pp. 843-855, September 1981.

8. N.G. Alexopoulos, P.B. Kathi and D.B. Rutledge, "Substrate optimization for integrated circuit antennas," IEEE Trans. Microwave Theory and Tech., Vol. MTT-31, pp. 550-557, July 1983.

9. B.S. Song and T. Itoh, "Distributed Bragg reflection dielectric waveguide oscillators," IEEE Trans. Microwave Theory Tech., Vol. MTT-27, pp. 1019-1022, Dec. 1979.

10. W.-B. Zhou and T. Itoh, "Analysis of trapped image guides using effective dielectric constant and surface impedances," IEEE Trans. Microwave Theory Tech., Vol. MTT-30, pp. 2163-2166, Dec. 1982.

11. W.-B. Zhou and T. Itoh, "Field distribution in the trapped image guide," Electromagnetics, Spring 1984.

12. J.-F. Miao and T. Itoh, "Hollow image guide and overlayed image guide coupler," IEEE Trans. Microwave Theory Tech., Vol. MTT-30, pp. 1826-1831, Nov. 1982.

13. J.-F. Miao and T. Itoh, "Coupling between microstrip line and

image guide through small apertures in the common ground plane," IEEE Trans. Microwave Theory Tech., Vol. MTT-31, pp. 361-363, April 1983.

14. A.R. Kerr, P.H. Siegel and R.J. Mattanch, "A simple quasi-optical mixer for 100-120 GHz," 1979 IEEE MTT-S International Microwave Symposium, pp. 96-98, San Diego, CA., June 21-23, 1977.

15. K.D. Stephan, N. Camilleri and T. Itoh, "A quasi-optical polarization-duplexed balanced mixer for millimeter-wave applications," IEEE Trans. Microwave Theory and Tech., Vol. MTT-31, pp. 164-170, February 1983.

16. K.D. Stephan and T. Itoh, "A planar quasi-optical subharmonic mixer characterized by isotropic conversion loss," IEEE Trans. Microwave Theory and Tech., Vol. MTT-31, January 1984.

17. K.D. Stephan and T. Itoh, "An inexpensive short-range microwave telemetry transponder," to be published.

18. R. Mittra and S.W. Lee, Analytical Techniques in the Theory of Guided Waves, New York, Macmillan, 1971.

19. G.F. Vanblaricum, Jr. and R. Mittra, "A modified residue-calculus technique for solving a class of boundary value problems-Part II: Waveguide phased arrays, modulated surfaces and diffraction gratings, IEEE Trans. Microwave Theory Tech., Vol. MTT-17, pp. 310-319, June 1969.

20. Y.C. Shih, T. Itoh and L.Q. Bui, "Computer-aided design of millimeter-wave E-plane filters," IEEE Trans. Microwave Theory and Tech., Vol. MTT-31, pp. 135-142, February 1983.

21. L.Q. Bui, D. Ball and T. Itoh, "Broadband millimeter-wave E-plane bandpass filters," 1984 IEEE MTT-S International Microwave Symposium, pp.236-237, San Francisco, CA, May 30-June 1, 1984.

22. J.D. Rhodes, Theory of Electrical Filter, New York, John Wiley & Sons, 1976.

23. J. Rivera and T. Itoh, "Analysis of an electromagnetically coupled patch antenna," 1983 International Anntennas and Propagation Symposium, Vol. 1, pp. 170-173, Houston, TX, May 23-26, 1983.

24. Q. Zhang, Y. Fukuoka, T. Itoh and L. Su, "Analysis of a suspended patch antenna excited by an electromagnetically coupled inverted microstrip feed," to be presented at European Microwave Conference, Liege, Belgium, Sept. 10-13, 1984.

25. L. Su, T. Itoh, and J. Rivera, "Design of an overlay directional coupler by a full-wave analysis," IEEE Trans. Microwave Theory and Tech., Vol. MTT-31, pp. 1017-1022, December 1983.

26. A. Beyer, "Calculation of discontinuities in grounded finlines taking into account the metallization thickness and the influence of the mount-slits," 12th European Microwave Conference, pp. 681-686, Helsinki, Finland, September 1982.

27. R. Sorrentino and T. Itoh, "Transverse resonance analysis of finline discontinuities," 1984 IEEE MTT-S International Microwave Symposium, pp. 414-416, San Francisco, CA, May 30-June 1, 1984.

28. T. Sakurai, "Approximation of wiring delay in MOSFET LSI," IEEE Solid State Circuits, Vol. SC-18, No. 4, August 1983.

29. H.-T. Yuan, Y.-T. Lin and S.-Y. Chiang, "Properties of interconnection on silicon, sapphire and semi-insulating Gallium Arsenide substrate," IEEE Solid State Circuits, Vol. SC-17, No. 2, April 1982.

30. Y. Fukuoka, Q. Zhang, D. Neikirk and T. Itoh, "Analysis of multilayer interconnection lines for a high speed digital integrated circuit," First International IEEE VLSI Multilevel Interconnection Conference, pp. 246-251, New Orleans, LA, June 21-22, 1984.

31. B. Bayraktaroglu and H.D. Shih, "Millimeter-wave GaAs distributed IMPATT diodes," IEEE Electron Devices Lett., Vol. EDL-4, pp. 393-395, Nov. 1983.

32. Y. Fukuoka and T. Itoh, "Field analysis of millimeter-wave GaAs double-drift IMPATT diode in the travelling wave mode," 1984 IEEE MTT-S International Microwave Symposium, pp. 169-171, San Francisco, CA, May 30-June 1, 1984.

33. H. Hasegawa and H. Okizaki, "M.I.S. and Schottky slow-wave coplanar striplines on GaAs substrate," Electron. Lett., Vol. 13, pp. 663-664, Oct. 1979.

34. Y. Fukuoka and T. Itoh, "Coplanar Schottky variable phase shifter constructed on GaAs substrate for millimeter-wave application," International J. Infrared and Millimeter Waves, Vol. 5, pp. 793-801, June 1984.

List of Personnel

Principal Investigator

T. Itoh

Faculty Associate

D.P. Neikirk

Research Associates

K.D. Stephan
Y. Fukuoka

Visiting Scholar

R. Sorrentino

Research Fellows

J.F. Miao
W. Zhou
L. Su

Research Assistants/Students

J. Rivera
Y. Shih
N. Camilleri
M. Debner
N.U. Song
Q. Zhang

Degrees Awarded

Master of Science	N. Camilleri	May 1982
	Q. Zhang	May 1984
Ph.D.	Y. Shih	August 1982
	J. Rivera	December 1982
	K.D. Stephan	May 1983
	Y. Fukuoka	May 1984

Publications Under ARO Support (April 1981-date)

1. "Characteristics of unilateral fin-line structures with arbitrarily located slots," IEEE Trans Microwave Theory and Tech., Vol. MTT-29, No. 4, pp. 352-355, April 1981 (L.P. Schmidt and T. Itoh).

2. "Characteristics of a generalized fin-line for millimeter-wave integrated circuits," International J. Infrared and Millimeter Waves, Vol. 2, No. 3, pp. 427-436, May 1981 (L.P. Schmidt and T. Itoh)

3. "An analysis of distributed Gunn effect devices with subcritical doping," International J. Infrared and Millimeter Waves, Vol. 2, No. 5, pp. 883-904, September 1981 (I. Awai and T. Itoh).

4. "Trapped image guide leaky-wave antenna for millimeter wave applications," IEEE Trans. Antennas and Propagation, Vol. AP-30, No. 3, pp. 505-509 (T. Itoh and B. Adelseck).

5. "Analysis of conductor-backed coplanar waveguide," Electronics Letters, Vol. 18, No. 12, pp. 538-540, June 10, 1982 (Y.C. Shih and T. Itoh).

6. "Analysis of printed transmission lines for monolithic integrated circuits," Electronics Letters, Vol. 18, No. 14, pp. 585-586, July 18, 1982 (Y. Shih and T. Itoh).

7. "Analysis of printed transmission lines for monolithic integrated circuits," Electronics Letters, Vol. 18, No. 14, pp. 585-586, July 18, 1982 (Y. Shih and T. Itoh)

8. "Open guiding structures for millimeter-wave integrated circuits," Microwave Journal, Vol. 25, No. 9, pp. 113-126, September 1982.

9. "Hollow image guide and overlayed image guide coupler," IEEE Trans. Microwave Theory and Tech., Vol. MTT-30, No. 11, pp. 1826-1831, November 1982 (J.-F. Miao and T. Itoh).

10. "Analysis of trapped image guide using effective dielectric constants and surface impedance," IEEE Trans. Microwave Theory and Tech., Vol. MTT-30, No. 12, pp. 2163-2166, December 1982 (W.B. Zhou and T. Itoh).

11. "Slow-wave propagation in MIS periodic coplanar waveguide," Electronics Letters, Vol. 19, No. 2, pp. 37-38, January 20, 1983 (Y. Fukuoka and T. Itoh).

12. "Computer-aided design of millimeter-wave E-plane filters," IEEE Trans. Microwave Theory and Tech., Vol. MTT-31, No. 2, pp. 135-

142, February 1983 (Y. Shih, T. Itoh and L.Q. Bui).

13. "A quasi-optical polarization-duplexed balanced mixer for millimeter-wave applicatons," IEEE Trans. Microwave Theory and Tech., Vol. MTT-31, No. 2, pp. 164-170, February 1983 (K.D. Stephan, N. Camilleri and T. Itoh).

14. "Coupling between microstrip line and image guide through small apertures in the common ground plane," IEEE Trans. Microwave Theory and Tech., Vol. MTT-31, No. 4, pp. 361-363, April 1983 (J.-F. Miao and T. Itoh).

15. "Analysis of slow-wave coplanar waveguide for monolithic integrated circuits," IEEE Trnas. Microwave Theory and Tech., Vol. MTT-31, No. 7, 567-573, July 1983 (Y. Fukuoka, Y.C. Shih and T. Itoh).

16. "Slow-wave coplanar waveguide on periodically doped semiconductor substrates," IEEE Trans. Microwave Theory and Tech., Vol. MTT-31, Nov. 12, pp. 1013-1017, December 1983 (Y. Fukuoka and T. Itoh).

17. "Design of an overlay directional coupler by a full-wave analysis," IEEE Trans. Microwave Theory and Tech., Vol. MTT-31, No. 12, pp. 1019-1022, December 1983, (L. Su, T. Itoh and J. Rivera).

18. "E-plane filters with finite-thickness septa," IEEE Trans. Microwave Theory and Tech., Vol. MTT-31, No. 12, pp. 1009-1013, December 1983, (Y. Shih and T. Itoh).

19. "A planar quasi-optical subharmonic mixer characterized by isotropic conversion loss," IEEE Trans. Microwave Theory and Tech., (K.D. Stephan and T. Itoh).

20. "Analysis of an electromagnetically coupled patch antenna," Electromagnetics, Vol. 3, No. 4, October 1983, (J. Rivera and T. Itoh).

21. "Analysis of an electromagnetically coupled patch antenna," Electromagnetics, Vol. 4, No. 1, January 1984, (W. B. Zhou and T. Itoh).

22. "Coplanar Schottky variable phase shifter constructed on GaAs substrate for millimeter-wave application," International J. Infrared and Millimeter Waves, Vol. 5, No. 6, pp. 793-801, June 1984 (Y. Fukuoka and T. Itoh).

Conference Presentations under ARO Support

1. "Directive planar excitation of an image-guide," 1981 IEEE MTT-S International Microwave Symposium, June 15-18, 1981, Los Angeles, CA, pp. 114-116, (Y. C. Shih, J. Rivera and T. Itoh).

2. "Open guided wave structures for millimeter-wave circuits," (Invited), 1981 IEEE MTT-S International Microwave Symposium, June 15-18, 1981, Los Angeles, CA, pp. 114-116 (P. Yen, J.A. Paul and T. Itoh).

3. "Millimeter-wave planar slot antennas with dielectric feeds," 1981 IEEE MTT-S International Microwave Symposium, June 15-18, 1981, Los Angeles, CA, pp. 114-116 (P. Yen, J.A. Paul and T. Itoh).

4. "Planar dielectric waveguides and other surface-wave structures," XXth General Assembly, International Union of Radio Science, August 10-19, 1981, Wasington, D.C., p. 183 (T. Itoh).

5. "Recent advances in dielectric millimeter-wave integrated circuits," SPIE Symposium on Integrated Optics and Microwave Integrated Circuits, November 16-19, 1981, Huntsville, AL, pp. 211-218 (T. Itoh).

6. "Open guided wave structures for millimeter-wave integrated circuits," IEEE International Symposium on Circuits and Systems, May 10-12, 1982, Rome Italy, pp. 957-959 (T. Itoh).

7. "Analysis of trapped image guides using effective dielectric constants and surface impedances," 1982 IEEE MTT-S International Microwave Symposium, June 14-18, 1982, Dallas, Texas, pp. 295-297 (W.B. Zhou and T. Itoh).

8. "Computer-aided design of millimeter-wave E-plane filters," 1982 IEEE MTT-S International Microwave Symposium, June 14-18, 1982, Dallas, Texas, pp. 471-473 (Y.C. shih, T. Itoh, and L. Bui).

9. "Quasi-optical polarization-duplexed balanced mixer," 1982 IEEE MTT-S International Microwave Symposium, June 14-18, 1982, Dallas, Texas, pp. 376-378 (K.D. Stephan, N. Camilleri and T. Itoh).

10. "Hollow image guide for millimeter-wave integrated circuits," 12th European Microwave Conference, Helsinki, Finland, September 1982, pp. 520-525 (J.-F. Miao and T. Itoh).

11. "Analysis of printed transmission lines for monolithic integrated circuits," 12th European Microwave Conference, Helsinki, Finland, September 1982, pp. 520-525 (J.-F. Miao and T. Itoh).

12. "Analysis of an electromagnetically coupled patch antenna," 1983 International Symposium Digest Antennas and Propagation, Vol. 1, May 23-26, 1983, Houston, Texas, pp. 190-193, (J. Rivera and T. Itoh).

13. "E-plane filters with finite-thickness septa," 1983 International Microwave Symposium Digest, May 31-June 3, 1983, Boston, MA, pp. 157-159 (Y.C. Shih and T. Itoh).

14. "Slow-wave coplanar waveguide on periodically doped semiconductor substrates," 1983 International Microwave Symposium Digest, May 31-June 3, 1983, Boston, MA, pp. 399-401 (Y. Fukuoka and T. Itoh).

15. "Field distributions in the trapped image guide," 1983 International Microwave Symposium Digest, May 31-June 3, 1983, Boston, MA, pp. 227-229 (W.B. Zhou and T. Itoh).

16. "Design of an overlay directional coupler by a full-wave analysis," 1983 International Microwave Symposium Digest, May 31-June 3, 1983, Boston, MA, pp. 427-429 (L. Su, T. Itoh and J. Rivera).

17. "Quasi-optical planar mixers for millimeter-wave imaging applications," Proceedings of the SPIE, August 22-26, 1983, San Diego, CA (T. Itoh and K.D. Stephan).

18. "Design consideration of uniform and periodic coplanar Schottky variable phase shifter," 13th European Microwave Conference Proceedings, Sept. 5-8, 1983, Nurnberg, W. Germany, pp. 278-282 (Y. Fukuoka and T. Itoh).

19. "Isotropic conversion loss as a measure of quasi-optical mixer efficiency," 8th International Conf. on Infrared and Millimeter Waves, December 12-17, 1983, Miami Beach, FL, Paper No. TH3.3 (K.D. Stephan and T. Itoh).

20. "Recent development of dielectric waveguide technology," SPIE Technical Symposium East '84, April 29-May 4, 1984, Arlington, VA, Paper No. 477-14 (T. Itoh).

21. "Broadband millimeter-wave E-plane bandpass filters," 1984 IEEE MTT-S International Microwave Symposium, pp. 236-237, San Francisco, CA, May 30-June 1, 1983 (L. Bui, D. Ball and T. Itoh).

22. "Transverse resonance analysis of finline discontinuities," 1984 IEEE MTT-S International Microwave Symposium, pp. 414-416, San Francisco, CA, May 30-June 1, 1984 (R. Sorrentino and T. Itoh).

23. "Field analysis of millimeter-wave GaAs double-drift IMPATT diode in the travelling-wave mode," 1984 IEEE MTT-S International Microwave Symposium, pp. 169-171, May 30-June 1, 1984 (Y. Fukuoka

and T. Itoh).

24. "Analysis of multilayer interconnection lines for a high speed digital integrated circuit," First International IEEE VLSI Multilevel Interconnection Conference, pp. 246-251, New Orleans, LA, June 21-22, 1984 (Y. Fukuoka, Z. Zhang, D. Neikirk and T. Itoh).

Patent Application

Quasi-optical polarization duplexed balanced mixer

Technical Reports

1. "A study of microwave and millimeter-wave quasi-optical planar mixers," Microwave Laboratory Report No. 83-2, August 1983 (K.D. Stephand and T. Itoh).

2. "Computer-aided design of millimeter-wave E-plane filters," Microwave Laboratory Report No. 84-1, March 1984.

3. "Millimeter-wave travelling wave IMPATT diode," Microwave Laboration Reprot No. 84-6, May 1984

APPENDIX 1

A Quasi-Optical Polarization-Duplexed Balanced Mixer for Millimeter-Wave Applications

KARL D. STEPHAN, STUDENT MEMBER, IEEE, NATALINO CAMILLERI, STUDENT MEMBER, IEEE, AND TATSUO ITOH, FELLOW, IEEE

Abstract — **An integrated planar antenna-mixer structure for use at millimeter-wave frequencies is described. A simple but accurate theory of the slot-ring antenna is applied to several experimental devices. Mixer conversion loss of about 6.5 dB was obtained from an *X*-band model. Measured radiation patterns of structures designed for 65 GHz agree reasonably well with theory.**

I. Introduction

As millimeter-wave systems increase in complexity, a strong need arises to simplify each component to the utmost extent. What may be a practical size for a single receiver front end (antenna, mixer, and associated waveguides) becomes highly impractical if one tries to build an array of such receivers. The planar structure described in this paper combines the functions of receiving antenna and balanced mixer in one simple metallized pattern on a dielectric substrate, which indeed can be the semiconductor from which the mixer diodes are formed. A working model tested at *X*-band gave a conversion loss of 6.5 ± 3 dB, and actual devices designed for use above 30 GHz yielded antenna radiation patterns which agree with the theory developed in this paper. Detailed discussion of operation will begin with the antenna structure itself.

Manuscript received May 5, 1982; revised June 21, 1982. This work was supported by U.S. Army Night Vision and Electro-optics Laboratory through the U.S. Army Research Office under Contract DAAG29-81-K-0053.

The authors are with the Department of Electrical Engineering, University of Texas at Austin, Austin, TX 78712.

II. Slot-Ring Antenna

The slot-ring antenna is one of a class of radiating structures formed from a gap or hole in an otherwise continuous metallic sheet. The sheet may or may not be backed on one side by a dielectric layer. In this paper, both the conducting sheet and the dielectric are assumed to be lossless. The slot-ring structure is the mechanical dual of the more familiar microstrip-ring resonator (see Fig. 1). The microstrip ring is a segment of microstrip bent into a loop; the slot ring is a segment of slot line bent into a loop. Slot line, first described by Cohn [1], has recently found application in millimeter-wave mixers [2]. The technique of bonding mixer diodes across the slot results in a connection with minimum stray inductance. This advantage is utilized in the mixer to be described.

0018-9480/83/0200-0164$01.00 ©1983 IEEE

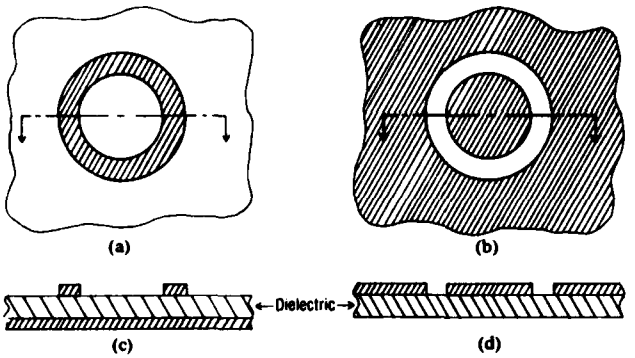

Fig. 1. Comparison of (a) microstrip-ring and (b) slot-ring structures. (c) Ground plane. (d) No ground plane.

Like the microstrip resonator, the slot-ring structure's resonant modes occur at frequencies for which the ring circumference equals an integral number of guide wavelengths. To use the structure as an antenna, the first-order mode is excited as shown in Fig. 2. Neglecting the other modes for the moment, the impedance seen by the voltage source will be real at resonance, and all the power delivered will be radiated. Three problems arise: 1) how to calculate the resonant frequency; 2) how to determine the ring's radiation pattern; and 3) how to find the input resistance at resonance.

A first-order estimate of the resonant frequency can be derived from the transmission line equivalent circuit of the slot ring (Fig. 3). By placing a magnetic wall across the ring as shown in Fig. 3(a), we disturb nothing since the structure is symmetrical. The wall permits opening the ring at the point diametrically opposite the feed, since no current flows through the wall. This operation yields the equivalent transmission-line circuit shown in Fig. 3(b).

At the resonant frequency of the first-order mode, the two lines are each a half-wave long electrically. Knowledge of the mechanical length (πr_{av}, where r_{av} is the average ring radius) and the velocity factor allows the calculation of resonance to within about 10 to 15 percent of the true frequency, even though the published tables for straight slot line [3] are used with the curved line shown in Fig. 3(a). The smaller the relative gap g/r_{av}, the better the estimate will be. For a more precise calculation, recourse can be made to spectral-domain techniques such as in the paper by Araki and Itoh [4]. Once the resonant frequency is determined for a particular application, both the radiation patterns and the impedance may be found by means of the following analysis.

In [4], Araki and Itoh showed that if the tangential electric field was known on a cylindrically symmetric planar surface, the field could be Hankel-transformed to derive the far-field radiation patterns from that surface. In their case, the fields had to be calculated from estimates of the currents on a microstrip patch. In the present case, however, a very simple estimate of the electric field in the slot will yield a good evaluation of the antenna patterns and the radiation impedance.

In choosing an estimate of the field, care should be taken to insure that the functional form is easy to Hankel-transform analytically. The estimate chosen is

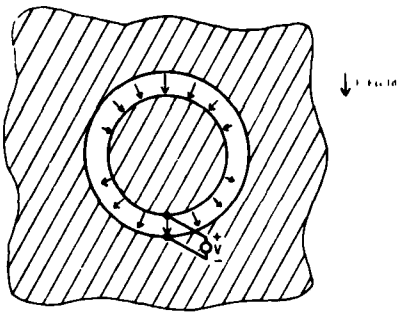

Fig. 2. Slot-ring feed method showing electric field in plane of device.

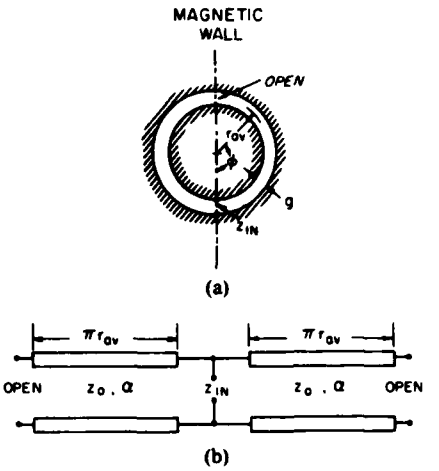

Fig. 3. Transmission-line equivalent circuit of slot-ring antenna. (a) With magnetic wall across slot ring. (b) Resulting transmission-line circuit.

$$E_r(r) = \frac{1}{r} \quad \text{for } \left(r_{av} - \frac{g}{2}\right) < r < \left(r_{av} + \frac{g}{2}\right) \tag{1}$$

$$E_r(r) = 0 \quad \text{otherwise} \tag{2}$$

$$E_\phi = 0. \tag{3}$$

This simple choice satisfies the boundary condition that the tangential electric field be zero on the metallic sheet, and expresses the intuitively reasonable idea that, for narrow gaps at least, the azimuthal field in the gap will be small compared to the radial field.

Define the $(n \pm 1)$th order Hankel transforms of the chosen function to be

$$\tilde{E}_{(\pm)}(\alpha) = \int_0^\infty E_r(r) J_{n\pm1}(\alpha r) r\, dr \tag{4}$$

where $J_n(\alpha r)$ is the nth-order Bessel function of the first kind, and α is the Hankel-transform variable. Applying this to the chosen estimate, we find

$$\tilde{E}_{(\pm)}(\alpha) = \int_{r_i}^{r_o} \frac{1}{r} J_{n\pm1}(\alpha r) r\, dr \tag{5}$$

$$\tilde{E}_{(\pm)}(\alpha) = \int_{r_i}^{r_o} J_{n\pm1}(\alpha r)\, dr \tag{6}$$

where we have called the inner and outer ring radii r_i and r_o, respectively. This integral is easy to evaluate analyti-

cally, through recursion relations given in published tables [5]. Assuming that all the fields vary as $e^{jn\phi}$, and using the saddle-point equations given in [3], we find that the far-field equations for E_θ and E_ϕ are

$$E_\theta(r,\theta,\phi) = -k_0 \frac{e^{-jk_0 r}}{r} \frac{j^n e^{jn\phi}}{2} \left[\tilde{E}_0(k_0 \sin\theta)\right] \tag{7}$$

$$E_\phi(r,\theta,\phi) = +k_0 \frac{e^{-jk_0 r}}{r} \frac{j^{n+1} e^{jn\phi}}{2} \cos\theta \left[\tilde{E}_e(k_0 \sin\theta)\right] \tag{8}$$

where linear combinations of the Hankel-transformed estimates are used

$$\tilde{E}_0(k_0 \sin\theta) = \tilde{E}_{(+)}(k_0 \sin\theta) - \tilde{E}_{(-)}(k_0 \sin\theta) \tag{9}$$

$$\tilde{E}_e(k_0 \sin\theta) = \tilde{E}_{(+)}(k_0 \sin\theta) + \tilde{E}_{(-)}(k_0 \sin\theta). \tag{10}$$

The standard spherical coordinates r, θ, and ϕ refer to the point at which the fields are measured, $r = 0$ being the center of the ring. The quantity k_0 is the wavenumber in free space $\omega\sqrt{\mu_0 \epsilon_0}$, and n is the order of resonance being analyzed. In the case of interest, $n = 1$ and $\omega = \omega_0$, the resonant frequency.

Equations (7) through (10) apply to any tangential electric field in the plane containing the origin of the spherical coordinate system. In order to treat the case of a finite thickness of dielectric, the estimated field must be transformed through the dielectric layer so that the Hankel transforms operate on the dielectric-air interface. In the Hankel-transform domain, this is a relatively easy process. Define d to be the thickness of the dielectric layer of relative dielectric constant ϵ_r.

If we let

$$\alpha = k_0 \sin\theta \tag{11}$$

$$\beta_1 = \sqrt{k_0^2 - \alpha^2} \tag{12}$$

$$\beta_2 = \sqrt{k_0^2 \epsilon_r - \alpha^2} \tag{13}$$

$$f_e(\alpha) = \frac{\beta_2 \cos\beta_2 d + j\epsilon_r \beta_1 \sin\beta_2 d}{\beta_2 \sin\beta_2 d - j\epsilon_r \beta_1 \cos\beta_2 d} \tag{14}$$

$$f_h(\alpha) = \frac{\beta_2 \sin\beta_2 d - j\beta_1 \cos\beta_2 d}{\beta_2 \cos\beta_2 d + j\beta_1 \sin\beta_2 d} \tag{15}$$

then the Hankel-transformed fields at the dielectric-air interface are given by

$$\tilde{E}_e(\alpha) = \left[\cos\beta_2 d + f_h(\alpha) \cdot \sin\beta_2 d\right] \cdot \left[\tilde{E}_{(+)}(\alpha) + \tilde{E}_{(-)}(\alpha)\right] \tag{16}$$

$$\tilde{E}_0(\alpha) = \left[\cos\beta_2 d - f_e(\alpha) \cdot \sin\beta_2 d\right] \left[\tilde{E}_{(+)}(\alpha) - \tilde{E}_{(-)}(\alpha)\right]. \tag{17}$$

Substituting these equations into (7) and (8) now gives the far-field expressions for the dielectric-coated side of the slot-ring antenna.

It should be noted that this analysis assumes that only the first-order mode is excited, and that no higher order surface waves arise. The former assumption is justified in that the zero-order mode and all higher order modes have a very small radiation impedance compared to that of the first-order mode, at its resonant frequency. The latter assumption may be justified [6] when the dielectric thickness is less than

$$d_{\max} = \frac{\pi}{2k_0\sqrt{\epsilon_r - 1}}. \tag{18}$$

Also, the equations assume that the metallic sheet extends to infinity. Practical antennas always stop short of this, but the effects of a noninfinite conductor will appear as inaccuracies only near $\theta = 90°$ (edge view of the device).

The third problem to be addressed is the radiation impedance. A classic method easily yields this result. The terminal voltage can be found by integrating the assumed field across the gap

$$|V| = \int_{r_i}^{r_a} \frac{1}{r} dr \tag{19}$$

$$|V| = \ln\left(\frac{r_a}{r_i}\right). \tag{20}$$

The total power radiated from the antenna with this voltage at its terminals is obtained [7] with the aid of (7) and (8)

$$P = \iint_{\text{sphere}} \frac{\frac{1}{2}\sqrt{|E_\theta|^2 + |E_\phi|^2}}{Z_{fs}} ds \tag{21}$$

where Z_{fs} is the intrinsic impedance of free space.

Since the input impedance Z_{in} at resonance is purely resistive, the input power at the terminals equals the radiated power

$$2 \cdot \frac{V^2}{2Z_{in}} = P. \tag{22}$$

The factor of 2 in front arises from the fact that the practical antenna is excited from only one point, but the field equations assume excitation of both orthogonal modes in quadrature ($\cos\theta + j\sin\theta$). Solving for Z_{in}, we find

$$Z_{in} = \frac{\left[\ln\left(\frac{r_a}{r_i}\right)^2\right]}{P}. \tag{23}$$

Care must be taken to use the proper equations for E_θ and E_ϕ on the dielectric and metal sides. This completes the analysis of the antenna. Strictly speaking, the resistance found in (23) applies only at the resonant frequency, although it will not vary appreciably for a small frequency range around resonance. The slot ring operated at its first-order resonance is a fairly low-Q device, so neither precise impedance calculations nor exact resonant frequencies are vital to a serviceable design.

III. Mixer Theory

Discussion of the mixer theory will be limited to explanations of the unique features embodied in the slot-ring antenna mixer.

The slot-ring antenna can support two independent

first-order modes, just as the microstrip ring resonator can. This feature allows a form of polarization duplexing in which two feed points, if separated by 90° along the ring, can couple independently to horizontally and vertically polarized waves, with little or no cross-coupling between the feeds. For exact independence, the two orthogonal feeds should each be balanced on diametrically opposite sides of the ring (four feed points altogether), but the slight imbalance caused by using only two feed points is small.

The basic operation of the mixer in a balanced, polarization-duplexed mode is illustrated in Fig. 4. The RF signal arrives as a horizontally polarized plane wave incident perpendicular to the antenna on the dielectric side. The LO signal is vertically polarized, and can arrive from either side of the structure. V_{rf} and V_{lo} show the electric field vectors on the antenna plane. By resolving each vector into two perpendicular components, it is easy to see that mixer diode D_1 receives

$$\frac{V_{lo} - V_{rf}}{\sqrt{2}}$$

while D_2 receives

$$\frac{V_{lo} + V_{rf}}{\sqrt{2}}.$$

In effect, each diode has its own independent mixer circuit, with the IF outputs added in parallel. The IF signal appears as a voltage between the central metal disc and the surrounding ground plane, and is removed through an RF choke. A double-balanced mixer with improved isolation can be made by adding two additional diodes D_3 and D_4, as indicated.

The diodes can be treated independently because each diode is at the zero-voltage node of the other diode's field pattern. To evaluate the impedance seen by a single diode, we can examine the nature of the impedance Z_{in} in Fig. 3(b). At the resonant frequency of the slot ring, the diode will see the antenna's radiation resistance, typically about 250 Ω. This impedance level is compatible with available diodes. At frequencies removed from resonance, the impedance presented to the diode will include reactance, but this variation is well-modelled by the transmission-line equivalent circuit up to the frequency at which the slot is no longer small compared to a wavelength. For narrow slots, this can be 10 to 20 times the operating frequency. In almost no other mixer structure is it so easy to calculate the impedance presented to the diode. Mixer performance is, of course, very dependent on the diode embedding impedance at RF and LO harmonic frequencies and combinations thereof. As the order of resonance increases, the slot ring becomes an increasingly poor radiating structure, so little power will be radiated in the form of higher harmonics.

The antenna-mixer can be introduced in a quasi-optical arrangement in its present form with good LO-to-RF isolation, because of the symmetry afforded by the balanced configuration. Additional improvement is easily achieved by introducing grid-type polarization filters on either side,

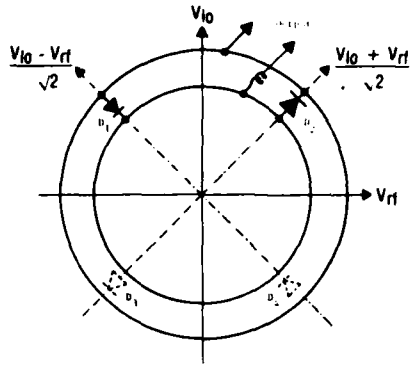

Fig. 4. Antenna-mixer showing diode input voltages.

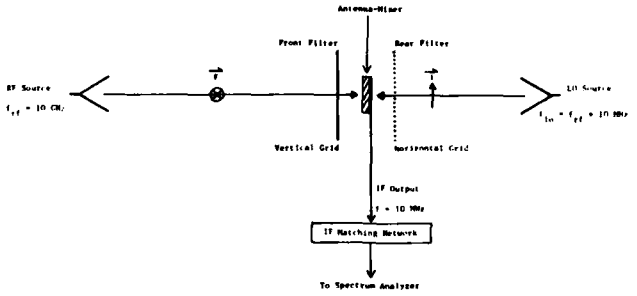

Fig. 5. Quasi-optical test setup.

as shown in Fig. 5. Horizontally polarized RF energy entering from the left passes through the front filter with little attenuation, and is received by the antenna. The rear filter is oriented to reflect the horizontally polarized RF wave, increasing directivity in the forward direction. Vertically polarized LO energy not absorbed by the antenna is blocked by the front filter and reflected back to the antenna, allowing a high degree of LO–RF isolation.

To summarize, polarization duplexing permits a balanced mixer configuration having inherently high LO-to-RF isolation. Diode embedding impedances are easy to calculate, and quasi-optical techniques can further enhance performance.

IV. Experiments

Various forms of the slot-ring structure have been constructed and measured at frequencies ranging from 400 MHz to 90 GHz. Due to equipment limitations, the only direct measures of impedance were limited to large structures below 1 GHz. These data are summarized in Table I. The calculated resonant frequencies were found using extrapolations of the published tables [3] for the $\epsilon_r = 12$ case. For the $\epsilon_r = 1$ cases, the average circumference was equated to the free-space wavelength for a first-order estimate, which turned out to be some 11-percent low. The radiation resistances were calculated using the experimentally derived resonant frequencies. Very good agreement was obtained for the $\epsilon_r = 1$ cases, and the 12-percent error for the $\epsilon_r = 12$ case is partly due to the poor mechanical contact between the metal foil used as the conducting sheet and the

TABLE I
SLOT-RING IMPEDANCE MEASUREMENTS

Structure Dimensions				Calculated Values		Measured Values		
Inner Radius (cm.)	Outer Radius (cm.)	Dielectric Constant (Relative)	Layer Thickness (cm.)	Resonant Frequency (MHz)	Radiation Resistance (ohms)	Resonant Frequency (MHz)	Radiation Resistance (ohms)	Radiation Q
7.7	8.2	1	--	600	240*	675±2	235±10	5
7.7	7.95	1	--	610	244*	676±2	232±10	6.6
3.048	3.302	12	0.635	720	590**	882±2	518±20	25.9

* At f_o = 660 MHz

** At f_o = 880 MHz

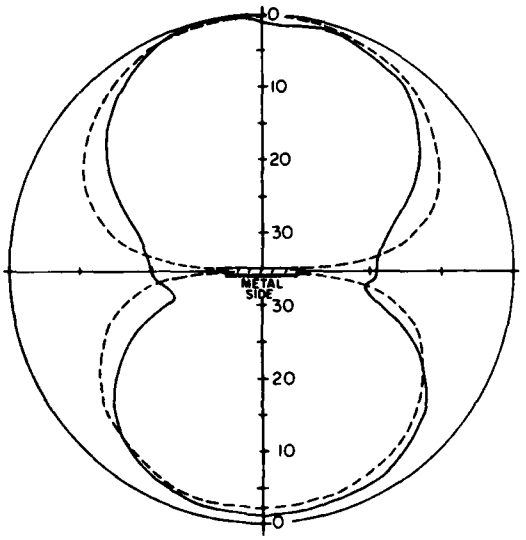

Fig. 6. Calculated and measured *H*-plane patterns, 10-GHz slot-ring antenna. Inner ring radius = 0.39 cm, outer ring radius = 0.54 cm, dielectric $\epsilon_r = 2.23$, thickness $d = 0.3175$ cm. All patterns are decibels down from maximum. --- Calculated.——Measured.

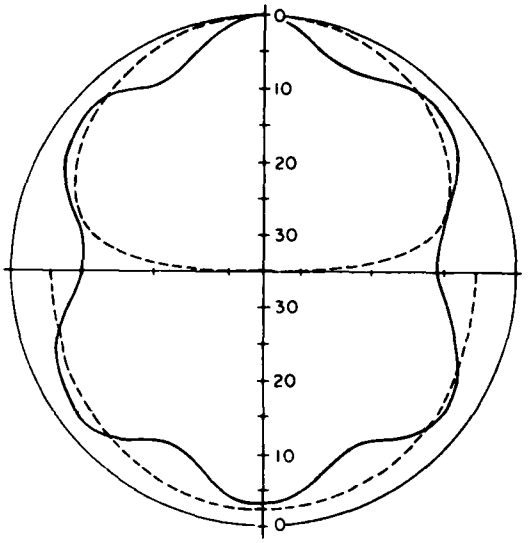

Fig. 7. Calculated and measured *E*-plane patterns, 10-GHz slot-ring antenna.

ceramic dielectric slab. Note that the radiation Q rises for the higher dielectric, but is still tolerably low even for a substrate having a dielectric constant near that of GaAs.

The next step taken was to build and measure a 10-GHz model antenna mixer. Calculated and measured antenna patterns are shown in Figs. 6 and 7. As anticipated, the predicted *H*-plane nulls in the plane of the device are partially filled in by attenuated surface waves. Overall agreement is good, especially the ratio of peak radiation intensity on the dielectric side to the metal side. An increase in either the resonant frequency or the dielectric constant will tend to pull the excitation currents to the dielectric side, increasing the field intensity there.

Using the measured antenna patterns for the 10-GHz model, an approximate directivity on the dielectric side was calculated to be 6.5 dB, which is typical of the rather broad patterns measured. The same antenna was then used to construct a balanced mixer of the type shown in Fig. 4. The mixer with its LO excitation was placed in an RF field of known intensity, and the directivity figure found above was used to calculate the actual RF power available to the mixer input, since direct measurement was impractical. The ratio of available RF input power to the measured IF output power delivered to a 10-MHz matching network gave the conversion loss reported in Table II. The 6.5 ± 3 dB figure compares not unfavorably to conventional mixer configurations. Depending on the effective diode impedance, this could be improved further with impedance-matching circuitry or different ring dimensions.

Owing to lack of a suitable local oscillator source, no actual mixer data is yet available in the millimeter-wave range, but extensive antenna patterns were measured with a single detector diode (HP 5082-2264) mounted on the ring feed point. Two different substrates were used. One was 0.3-mm-thick alumina, which was coated with a layer of gold about 2000 Å thick. Gold wire rings were used as masks to block the evaporation, forming the slot rings. The other substrate was a polymer compound with precoated copper on one side, removed mechanically to make rings. The antennas evaluated are specified in Table III, and illustrated in Figs. 8 and 9.

The alumina substrate was thin enough to avoid higher order surface waves at 65.2 GHz, its approximate design frequency. Calculated and measured patterns at this

Fig. 8. Alumina substrate mounted in antenna pattern setup.

Fig. 9 Diode on plastic substrate.

TABLE II
MEASURED ANTENNA-MIXER CHARACTERISTICS

Dimensions: Inner ring radius: 0.39 cm.
Outer ring radius: 0.54 cm.
Dielectric: 0.3175 cm. thick, $\epsilon_r = 2.23$

Diodes used: NEC ND4131 (R_b = 12 ohms)

Antenna-mixer system:

RF frequency: 10 GHz
IF frequency: 10 MHz
RF polarization: Horizontal
LO polarization: Vertical
Measured conversion loss: 8 dB ± 3 dB
LO-RF isolation: ≥ 30 dB
RF Cross-polarization rejection: 20 dB

TABLE III
MILLIMETER-WAVE ANTENNA DIMENSIONS

	Alumina Substrate	Plastic Substrate
Dielectric Constant	9.6	2.23
Inner Ring Radius	0.0325 cm.	0.045 cm.
Outer Ring Radius	0.0375 cm	0.070 cm.
Substrate Thickness	0.03 cm.	0.1588 cm.
Calculated Radiation Resistance	413 Ω at 65.2 GHz	390 Ω at 65.2 GHz
Substrate Size	2.9 cm. high 1.9 cm. wide	5 cm. square

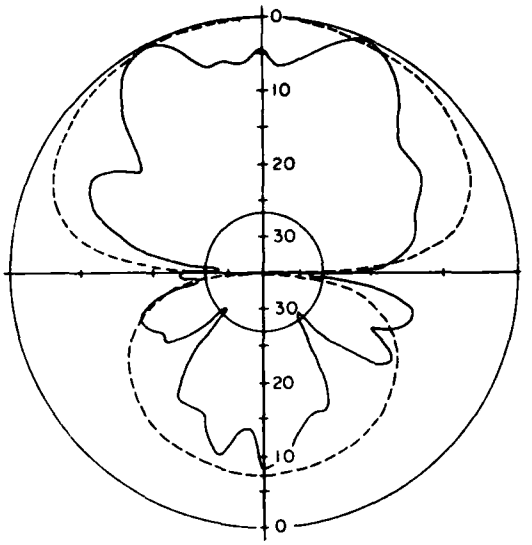

Fig. 10. Calculated and measured *H*-plane patterns, 65.2-GHz, alumina substrate. Circle indicates lower measurement limit, below which pattern is extrapolated.

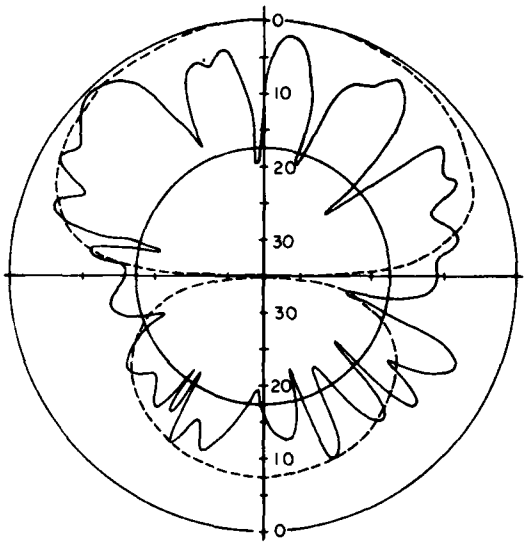

Fig. 11. Calculated and measured *H*-plane patterns, 95.5-GHz, alumina substrate.

frequency are shown in Fig. 10. Although the first-order mode radiation pattern does not predict the fine structure seen, prominent features such as the nulls in the plane of the device and the peak field values are predicted quite accurately. Compare this pattern to the one in Fig. 11, taken at 95.5 GHz. Higher order modes are evidently excited and surface waves have filled in the side nulls.

The plastic-substrate antenna was designed for 30 GHz, but equipment difficulties prevented pattern measurements in that range. The measurements of the same antenna at 65.2 GHz (Fig. 12) show effects of surface-wave excitation. The period of the nulls on the dielectric side is consistent with diffraction from the edges of the substrate itself, where surface waves emerge into the air.

Fig. 12 also shows that the feed method used does not interfere significantly with the radiation patterns. In all

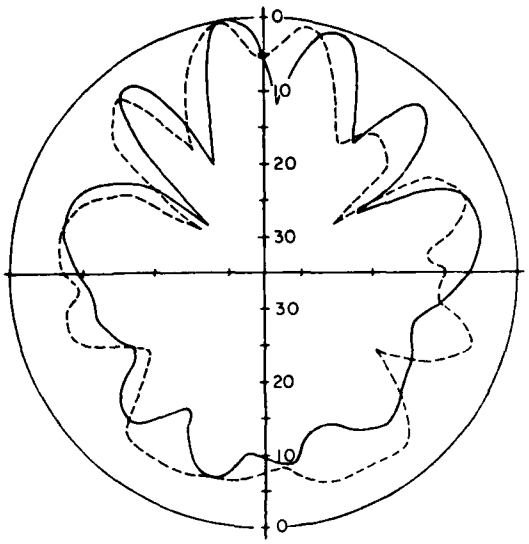

Fig. 12. Measured patterns, 65.2 GHz, plastic substrate. Dashed curve is without feed shield; solid curve is with feed shield.

other tests, the detected signal was removed from the central patch through a thin wire connected perpendicular to the device plane. After leading away from the antenna for 1–2 cm, the feed wire bends parallel to the substrate and leads to the output connector. The solid curve in Fig. 12 shows the effect of placing the insulated feed wire on the substrate and covering it with copper foil. The pattern change is relatively small, indicating that the original non-shielded feed was satisfactory. If the thin wire is not convenient mechanically, one alternative would be a coplanar line at IF, intersecting the central disc in the manner of a stick on a lollipop. A low-pass filter could be made of various sections of line with different impedances.

V. Conclusions

The slot-ring antenna-mixer has been shown to be a simple, practical component for use in quasi-optical receiving systems. A simple, but accurate, theory allows calculation of the radiation pattern and feed-point impedance, including effects of the dielectric layer. The performance of an *X*-band model was quite good for a first design attempt, and millimeter-wave measurements of structures on a high-dielectric-constant substrate indicate the practicality of forming such a device directly on a thin GaAs wafer. Arrays of such devices could open the way to phase-coherent imaging of millimeter-wave fields at a focal plane.

In addition to permitting image formation, arrays of devices will increase the overall system efficiency by presenting a larger effective aperture to typically large quasi-optical beams.

Acknowledgment

Thanks are due to L. Bui of Hughes Aircraft for providing the diodes used above 30 GHz, and to S. Sando of NEC for providing the *X*-band mixer diodes. J. Miller and Dr. R. Shurtz of the Army Night Vision and Electro-optics Laboratory provided the *X*-band detector diodes.

References

[1] S. B. Cohn, "Slot line on a dielectric substrate," *IEEE Trans. Microwave Theory Tech.*, vol. MTT-17, pp. 768–778, Oct. 1969.
[2] H. Ogawa, M. Akaike, M. Aikawa, T. Karaki, and J. Watanabe, "A 26-GHz band integrated circuit of a double-balanced mixer and circulators," *IEEE Trans. Microwave Theory Tech.*, vol. MTT-30, pp. 34–41, Jan. 1982.
[3] E. A. Mariani, C. P. Heinzman, J. P. Agrios, and S. B. Cohn, "Slot line characteristics," *IEEE Trans. Microwave Theory Tech.*, vol. MTT-17, pp. 1091–1096, Dec. 1969.
[4] K. Araki and T. Itoh, "Hankel transform domain analysis of open circular microstrip radiating structures," *IEEE Trans. Antennas Propagat.*, vol. AP-29, pp. 84–89, Jan. 1981.
[5] M. Abramowitz and I. Stegun, *Handbook of Mathematical Functions*. Washington, DC: U.S. Government Printing Office, 1972.
[6] R. F. Harrington, *Time-Harmonic Electromagnetic Fields*. New York: McGraw-Hill, 1961, p. 169.
[7] J. Kraus, *Antennas*. New York: McGraw-Hill, 1950, p. 28.

Karl D. Stephan (S'77–M'77–S'81) was born in Fort Worth, Texas, on December 18, 1953. He received the B.S. degree in engineering from the California Institute of Technology, Pasadena, CA, in 1976, and the M.Eng. Degree from Cornell University, Ithaca, NY, in 1977.

In 1977 he joined Motorola, Inc. in Fort Worth and worked in VHF and UHF mixer and filter design. From 1979 to 1981 he was with Scientific-Atlanta, Atlanta, GA, where he engaged in research and development pertaining to cable television systems. In 1981 he began graduate work at the University of Texas at Austin, where he is presently studying toward the Ph.D. degree.

Mr. Stephan is a member of Tau Beta Pi.

Natalino Camilleri (S'80) was born in St. Paul's Bay, Malta, on January 11, 1961. He received the B.Sc. honours degree in electrical engineering from the University of Malta in 1980, and the M.S.E. degree from the University of Texas at Austin in 1982.

He is now working as a Research Engineering Associate with the University of Texas. His current interests are low-noise millimeter-wave receivers and millimeter-wave integrated circuits.

Mr. Camilleri is a student member of IEE (London).

Tatsuo Itoh (S'69–M'69–SM'74–F'82) received the Ph.D. degree in electrical engineering from the University of Illinois, Urbana, in 1969.

From September 1966 to April 1976 he was with the Electrical Engineering Department at the University of Illinois. From April 1976 to August 1977 he was a Senior Research Engineer in the Radio Physics Laboratory, SRI International, Menlo Park, CA. From August 1977 to June 1978 he was an Associate Professor at the University of Kentucky, Lexington. In July 1978 he joined the faculty at the University of Texas at Austin, where he is now a Professor of Electrical Engineering and Director of the Microwave Laboratory. During the summer of 1979 he was a Guest Researcher at AEG-Telefunken, Ulm, West Germany.

Dr. Itoh is a member of the Institute of Electronics and Communication Engineers of Japan, Sigma Si, and Commission B of USNC/URSI. He serves on the Administrative Committee of the IEEE Microwave Theory and Techniques Society. He is a Professional Engineer registered in the State of Texas.

APPENDIX 2

Computer-Aided Design of Millimeter-Wave *E*-Plane Filters

YI-CHI SHIH, STUDENT MEMBER, IEEE, TATSUO ITOH, FELLOW, IEEE, AND L. Q. BUI

Abstract—A computer-aided design (CAD) algorithm has been developed for a class of *E*-plane bandpass filters. The analysis portion of the algorithm is based on the residue-calculus technique and a generalized scattering parameter method. It is mathematically exact and numerically very efficient. Filters designed with this method have been fabricated and tested in *Ka*-band. Good agreement with design has been obtained.

I. Introduction

SEVERAL FILTER CIRCUITS that are composed of a conductive sheet which is properly designed and sandwiched between the waveguide shells parallel to the *E*-plane have been proposed recently [1]–[5]. The circuits are developed either on a metal sheet [1], [2] or on a bilateral fin-line [3]–[5]. In these filters, the slot widths are equal to the waveguide height; thereby the structure really consists of several resonators separated by printed inductive strips. Since the structures, especially those in forms of fin-lines, are amenable to photolithographic techniques and only straight line shapes are involved, they are highly suitable for mass production. Some design procedures have been reported based on a number of methods such as mode-matching techniques and variational techniques. These methods have been applied only to metallic *E*-plane circuits or bilateral fin-line structures.

This paper presents a new efficient computer-aided design (CAD) algorithm developed for a class of *E*-plane bandpass filters. A unified treatment is introduced which applies not only to the purely metallic *E*-plane circuits and the bilateral fin-line circuits, but also to the unilateral and insulated fin-line circuits (Fig. 1). Since the analysis portion of the algorithm is based on the residue-calculus technique [6] and a generalized scattering parameter method [7], it is mathematically exact and numerically very efficient, as the convergence is guaranteed. Filters thus designed have been fabricated and tested in *Ka*-band with good agreement with the design.

II. Theory

The CAD program consists of an optimization routine and an analysis routine. We describe the analysis routine first. The analysis is carried out in three steps. First, a limiting case of a single junction created by a semi-infinite septum in a waveguide is analyzed. This structure may be analyzed exactly using the residue-calculus technique [6] to obtain a closed-form expression for the scattering matrix. The second step is to calculate the scattering parameters for a finite-length septum. This is done by placing two junctions back to back, and utilizing the concept of the generalized scattering matrix [7], which takes into account the interaction between junctions by not only the propagating modes but also all the evanescent modes. Finally, to combine several septums into a filter circuit, the generalized *S*-matrix technique is applied again to obtain the total scattering parameters of the composite structure.

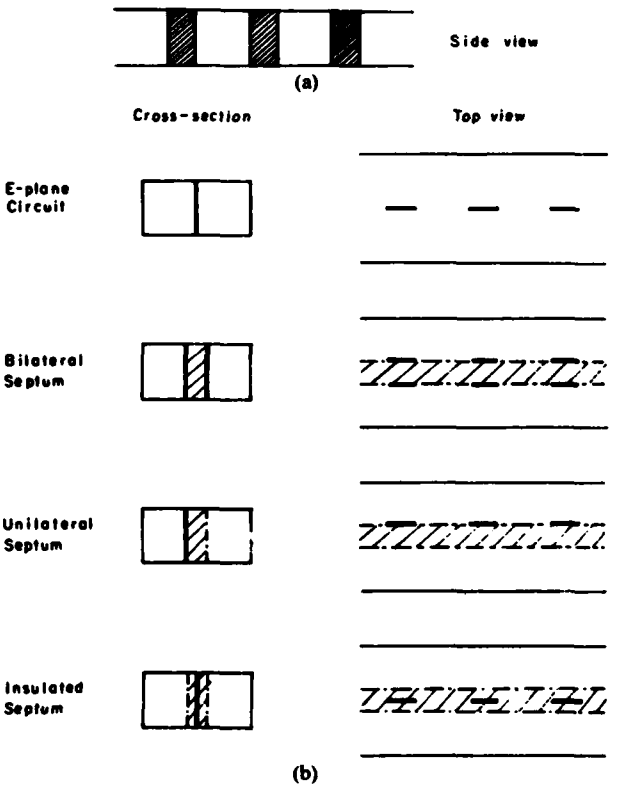

Fig. 1. Class of *E*-plane filter structures. (a) Side view. (b) Cross section and top view.

A. Semi-Infinite Septum

Let us consider an infinitesimally thin semi-infinite septum in a waveguide inhomogeneously filled with four

Manuscript received March 5, 1982; revised April 20, 1982. This work was supported in part by the U.S. Army Research Office Contract DAAG29-81-K-0053.

Y. C. Shih and T. Itoh are with the Department of Electrical Engineering, University of Texas, Austin, TX 78712.

L. Q. Bui is with the Hughes Aircraft Company, Electron Dynamics Division, Torrance, CA 90509.

0018-9480/83/0200-0135$01.00 ©1983 IEEE

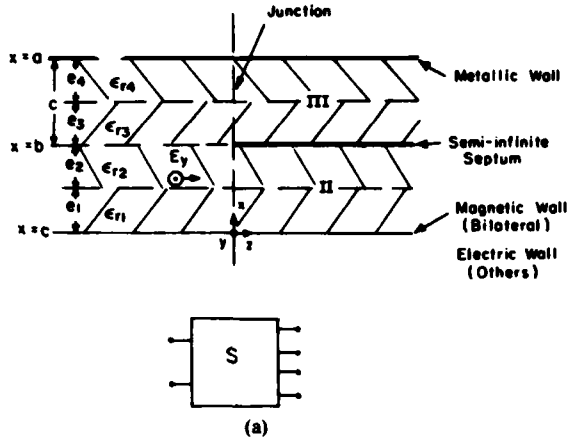

Fig. 2. Characterization of the edge of septum. (a) Geometry. (b) Matrix representation.

dielectric slabs as shown in Fig. 2(a). This is a generalized structure for which values of the thickness and dielectric constant of each layer can be chosen to represent the structures in Fig. 1(b). (Note that for the case of bilateral fin-lines, a magnetic wall is introduced at the center of the waveguide and only the region above the magnetic wall is considered. Such a region represents the upper half of the bilateral fin-line due to the symmetry of the structure.) It is then subdivided into three regions at the junction $z = 0$, with each region consisting of a uniform waveguide which possesses known eigenmodes and corresponding propagation constants.

Assuming a TE_{10}-type incident wave, the excited fields are composed of the TE_{no}-type waves since there are no structural variations in the y-direction. Therefore, the existing modal fields consist of only E_y, H_x, and H_z components. The total fields in each region are then expanded in terms of the eigenmodes. After matching the tangential field components at $z = 0$, and making use of the orthogonality of the eigenmodes, an infinite set of equations results. Since the existence of the stratified dielectric layer does not affect the edge condition of the septum, the equations are of the same form as that for a bifurcated waveguide described in [6] and the scattering parameters of the junction are obtainable by the residue-calculus technique.

The resulting scattering matrix has nine elements, each of which is also a matrix of infinite dimension. The terms in each element are of the form of an infinite product multiplied by some constant coefficient. They are summarized in the following:

$$S_{11}(m,p) = -\frac{H_p}{H_m} e^{-L(\gamma_m' + \gamma_p')} \frac{(\gamma_m'' - \gamma_m')(\gamma_m''' - \gamma_m')}{(\gamma_m'' + \gamma_p')(\gamma_m''' + \gamma_p')} \cdot f(m, -\gamma_m', \gamma_p') \quad (1a)$$

$$S_{21}(m,p) = \frac{H_p F_m}{2\gamma_m''} e^{L(\gamma_m'' - \gamma_p')} \frac{1}{(\gamma_m'' - \gamma_p')} \cdot f(0, \gamma_m'', \gamma_p') \quad (1b)$$

$$S_{31}(m,p) = \frac{H_p G_m}{2\gamma_m'''} e^{L(\gamma_m''' - \gamma_p')} \frac{1}{(\gamma_m''' - \gamma_p')} \cdot f(0, \gamma_m''', \gamma_p') \quad (1c)$$

$$S_{12}(m,p) = -\frac{H_m F_p}{2\gamma_m'} e^{L(\gamma_p'' - \gamma_m')} \frac{1}{(\gamma_m' - \gamma_p'')} \cdot f(0, \gamma_p'', \gamma_m') \quad (1d)$$

$$S_{22}(m,p) = -\frac{F_p}{F_m} e^{L(\gamma_m' + \gamma_p'')} \frac{(\gamma_m''' + \gamma_p'')(\gamma_m' - \gamma_m'')}{(\gamma_m''' - \gamma_m'')(\gamma_m' + \gamma_p'')} \cdot f(m, \gamma_p'', -\gamma_m'') \quad (1e)$$

$$S_{32}(m,p) = -\frac{F_p}{G_m} e^{L(\gamma_m''' + \gamma_p'')} \frac{(\gamma_m'' + \gamma_p'')(\gamma_m' - \gamma_m''')}{(\gamma_m'' - \gamma_m''')(\gamma_m' + \gamma_p'')} \cdot f(m, \gamma_p'', -\gamma_m''') \quad (1f)$$

$$S_{13}(m,p) = -\frac{H_m G_p}{2\gamma_m'} e^{L(\gamma_p''' - \gamma_m')} \frac{1}{(\gamma_m' - \gamma_p''')} \cdot f(0, \gamma_p''', \gamma_m') \quad (1g)$$

$$S_{23}(m,p) = -\frac{G_p}{F_m} e^{L(\gamma_m'' + \gamma_p''')} \frac{(\gamma_m''' + \gamma_p''')(\gamma_m' - \gamma_m'')}{(\gamma_m''' - \gamma_m'')(\gamma_m' + \gamma_p''')} \cdot f(m, \gamma_p''', -\gamma_m'') \quad (1h)$$

$$S_{33}(m,p) = -\frac{G_p}{G_m} e^{L(\gamma_m''' + \gamma_p''')} \frac{(\gamma_m'' + \gamma_p''')(\gamma_m' - \gamma_m''')}{(\gamma_m'' - \gamma_m''')(\gamma_m' - \gamma_p''')} \cdot f(m, \gamma_p''', -\gamma_m''') \quad (1i)$$

where

$$L = \frac{b}{\pi} \ln\left(\frac{a}{b}\right) + \frac{c}{\pi} \ln\left(\frac{a}{c}\right)$$

$$f(m, \gamma_1, \gamma_2) = \prod_{\substack{n=1 \\ n \neq m}}^{\infty} \frac{(\gamma_n' + \gamma_2)(\gamma_n'' + \gamma_1)(\gamma_n''' + \gamma_1)}{(\gamma_n' + \gamma_1)(\gamma_n'' + \gamma_2)(\gamma_n''' + \gamma_2)}$$

where γ_i', γ_i'', and γ_i''' are the propagation constants of the ith mode in Regions I, II, and III, respectively. F_i, G_i, and H_i are parameters determined readily for a given structure (see Appendix I). The notation $S_{ij}(m, p)$ stands for the scattering coefficient of the mth order mode.

B. Septum with Finite Length

With the knowledge of the scattering parameters for a single junction, the generalized scattering matrix technique is applied to obtain a two-port scattering matrix as

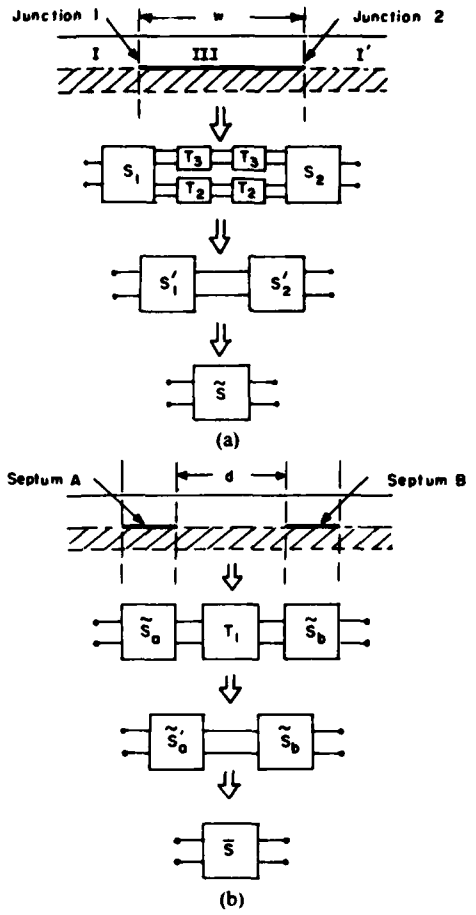

Fig. 3. *S*-parameter derivation. (a) For a single septum. (b) Cascaded septum.

shown in Fig. 3(a). Suppose now that the TE-type wave from Region I is incident upon Junction 1. At this junction, fields are reflected back into Region I, and transmitted into Regions II and III. After traveling a distance w, part of the wave transmitted into Regions II and III is reflected back and part is transmitted into Region I' at Junction 2. This process continues until the intensity of the reflected wave dies out. The multiple-reflection phenomenon between Junctions 1 and 2 is implied in a matrix manipulation which yields the scattering matrix for a finite length septum.

Referring to Fig. 3(a), S_1 and S_2 represent the scattering matrices for isolated Junctions 1 and 2 (i.e., for semi-infinite septums), respectively. From (1), we obtain the value of the elements in both matrices. Since the characteristics of these two junctions are essentially the same except for the opposite orientation, we have

$$S_2 = S_1^T. \tag{2}$$

We now define the transmission matrix

$$T = \begin{bmatrix} [I] & [0] & [0] \\ [0] & [T_2] & [0] \\ [0] & [0] & [T_3] \end{bmatrix} \tag{3}$$

where $[I]$ and $[0]$ are the identity matrix and the zero matrix, respectively, and the matrices $[T_2]$ and $[T_3]$ are of infinite size and represent the wave propagating (for propagation modes) or attenuating (for evanescent modes) for a distance of $w/2$ in guided Regions II and III, respectively. The combination of the transmission matrix along with S_1 and S_2 results in S_1' and S_2'

$$S_1' = TS_1T \tag{4}$$

$$S_2' = TS_2T = S_1^T. \tag{5}$$

A further combination of S_1' and S_2' then yields the composite scattering matrix $\tilde{S}$ for the septum of length w, viewed from I at $z = 0$ and from I' at $z = w$.

C. Filter Structures

For the final step of the analysis, several finite length septums are cascaded with appropriate separations to form a filter circuit. This is done by using the same techniques used in Section II-B described above. The procedure depicted in Fig. 3(b) shows the cascading of two septums represented by $\tilde{S}_a$ and $\tilde{S}_b$. The combination of $\tilde{S}_a$ and the transmission matrix T_1 results in matrix $\tilde{S}_a'$ which is further combined with $\tilde{S}_b$ to yield $\bar{S}$, the total scattering matrix of two septums with a separation of d. This procedure may be repeated to obtain the scattering parameters of a filter consisting of any number of septums.

III. Design

Based on the above analysis, a computer program is developed to calculate the total scattering parameters for a filter structure with given design parameters. Although the analysis is formally exact, in practice the infinite product in (1) and the infinite dimension of the elements in the scattering matrices need to be truncated. To obtain a very accurate result for (1), at least 300 terms should be retained. The calculation of the products here is efficient, since only readily known propagation constants are involved. Furthermore, this equation needs to be evaluated only once for a design assignment at each frequency point, since the scattering parameters of the semi-infinite septum depend only on the waveguide size and dielectric properties which are constant factors in a design.

For most applications, the fundamental mode is below cutoff in the narrow waveguide section and all of the higher order modes are evanescent in the wide waveguide. Therefore, only the first few accessible modes [8] are essentially responsible for the coupling between resonators. For most cases, only two or three modes are required to describe accurate scattering behavior. Notice that the number of modes considered here indicates the dimension of the matrices to be manipulated. The calculation includes a number of complex matrix multiplications and inversions. This analysis is efficient mainly due to the fact that only two or three modes are required.

Based on the analysis program, an optimization computer program applying the quasi-Newton method [9] is used which varies the input parameters until a desired

value of the insertion loss for a given bandwidth is obtained. To do this, an error function $F(\bar{x})$ to be minimized is defined

$$F(\bar{x}) = \sum_{N_s}\left(\frac{L_s}{|S_{21}|}\right)^2 + \sum_{N_p}\left(\frac{|S_{21}|}{L_s}\right)^2 \tag{6}$$

where N_s and N_p are the number of frequency sampling points in the stopband and passband, respectively, L_s and L_p are the minimum stopband and maximum passband attenuation levels, respectively, and $|S_{21}|$ is the calculated value of the filter attenuation. For a given thickness of the dielectric, the parameters $\bar{x}$ to be optimized are the septum lengths and resonator lengths.

To prevent the program from approaching nonrealizable or nonphysical results, upper and lower bounds of each parameter are specified

$$x_{li} < x_i < x_{ui}. \tag{7}$$

The constrained parameters are then reduced into essentially unconstrained ones by the transformation [10]

$$x_i = x_{li} + \frac{1}{\pi}(x_{ui} - x_{li})\cot^{-1}x_i' \tag{8}$$

where $-\infty < x_i' < \infty$, but only solutions within the range

$$0 < \cot^{-1}x_i' < \pi \tag{9}$$

are allowed. This transformation has a penalizing effect upon the parameters in the vicinity of the upper and lower bounds.

For the optimization procedure, the first two modes in each subregion are considered; the final design values are calculated with three modes. The total computing time for optimizing a five-resonator filter was about 2 min on a CDC Dual Cyber 170/750.

IV. Results and Discussion

In an earlier publication [11], it has been pointed out that the Q-factor of insulated fin-lines is inferior to that of bilateral fin-lines. Therefore, in this study, bandpass filters have been designed using only bilateral and unilateral fin-line configurations. Some typical designs for *Ka*-band applications are shown in Figs. 4, 6, and 7 fabricated on RT/Duroid substrates. Notice that the resonators are very weakly coupled by wide septums. In such cases, the septum cannot be represented by simple shunt-inductance equivalent circuits. Instead, it has to be represented by an equivalent T network [1]. Since the equivalent circuits are useful in conventional circuit design and are helpful for good initial guesses in the optimization procedure, this topic is discussed briefly in Appendix II.

The five-resonator filter design in Fig. 4 is a bilateral fin-line in which the hatched portion indicates metal on both sides of the substrate. The center frequency is 38.85 GHz, the 0.1-dB ripple bandwidth is 1.1 GHz, and the skirt selectivity at 500 MHz away from either edge of the passband is −40 dB. Measured characteristics of this filter are shown in Fig. 5. Computed responses are also plotted for comparison. Shapes of the calculated and measured

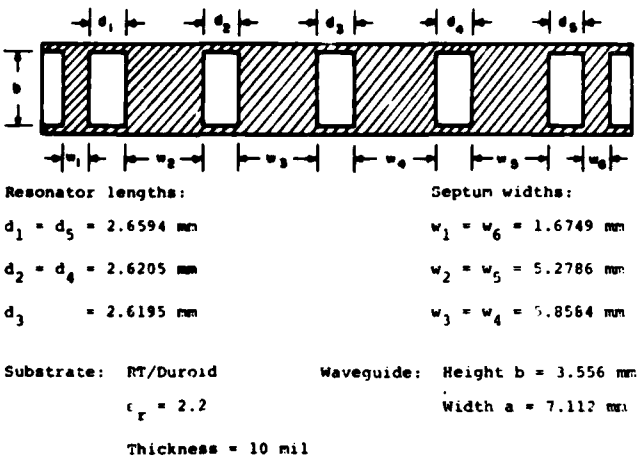

Fig. 4. Design example (five-resonator *Ka*-band bilateral fin-line filter).

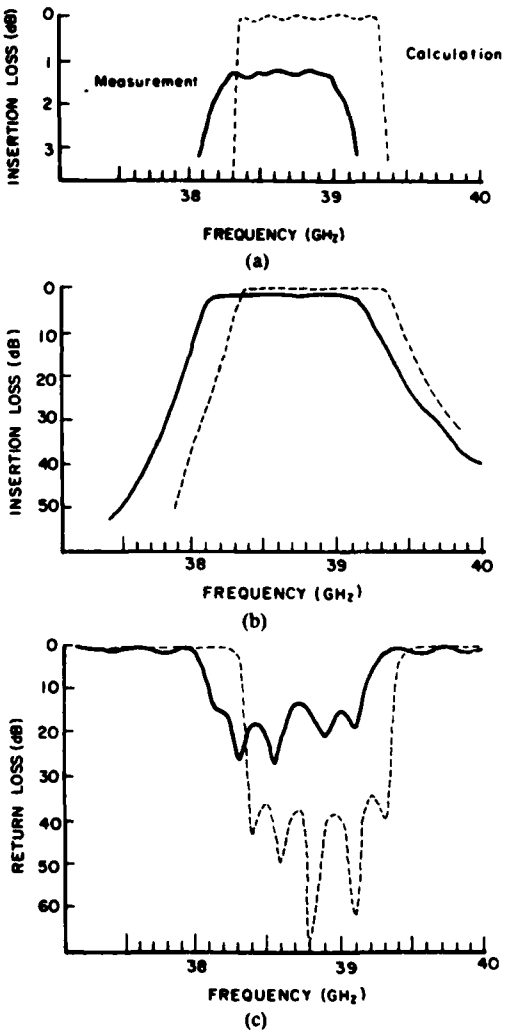

Fig. 5. Frequency responses for the filter in Fig. 4. (a) Expanded view of insertion loss. (b) Insertion loss characteristics. (c) Return loss characteristics.

response curves agree extremely well. Measured insertion loss in the passband is less than 1.3 dB of which 0.3 dB is associated with the test fixture. The measured center

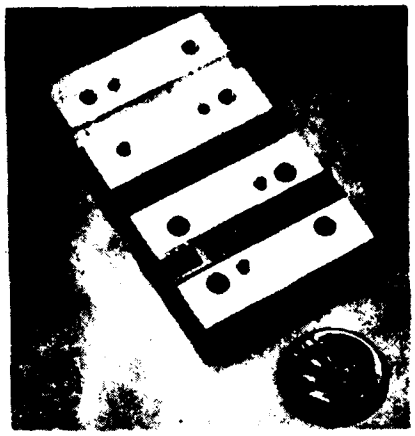

Fig. 6. Three-resonator *Ka*-band bilateral fin-line filter. Resonator length: $d_1 = d_3 = 2.6559$ mm; $d_2 = 2.6187$ mm. Septum width: $w_1 = w_4 = 1.7230$ mm; $w_2 = w_3 = 5.3628$ mm.

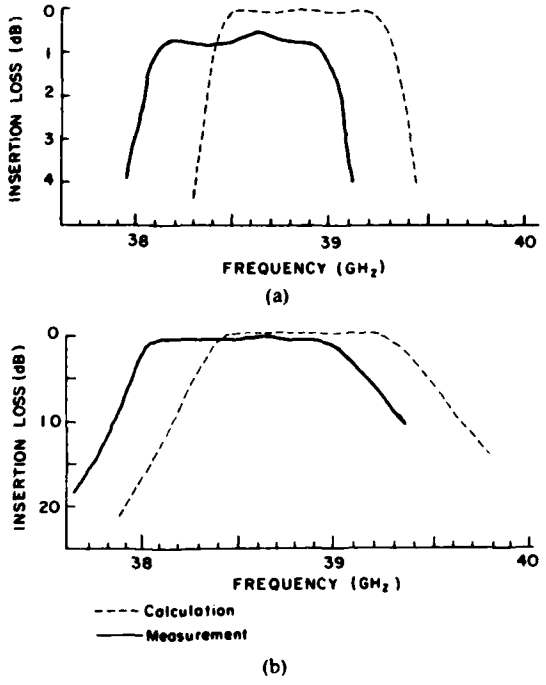

Fig. 7. Frequency responses for the filter in Fig. 6. (a) Expanded view of insertion loss. (b) Insertion loss characteristics. --- Calculation. —— Measurement.

frequency is shifted to the lower side by about 170 MHz which is less than 0.5 percent of the center frequency.

Fig. 6 shows a photograph of a three-resonator *Ka*-band bilateral fin-line filter printed on a 10-mil-thick RT/Duroid substrate. The design specifications for this filter were the same as those for the last one except for a decreased skirt selectivity of −20 dB. The measured results in Fig. 7 show that the insertion loss is less than 0.8 dB in the passband, including the fixture loss. The calculated and measured frequency responses again agree well; however, the measured center frequency is shifted down by about 300 MHz.

Bandpass filters have also been developed in unilateral fin-line configurations. A typical design for a three-resonator filter has the following specifications and dimensions:

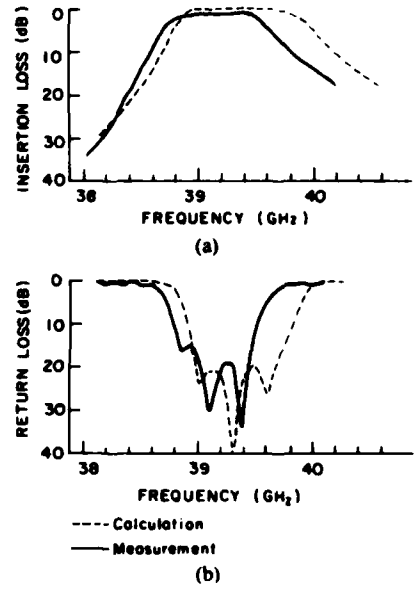

Fig. 8. Three-resonator *Ka*-band unilateral fin-line filter. --- Calculation. —— Measurement.

Resonator lengths	$d_1 = d_3 = 2.1568$ mm, $d_2 = 2.0879$ mm;
Septum widths	$w_1 = w_4 = 2.3325$ mm, $w_2 = w_3 = 6.8718$ mm;
Passband	39.0 ~ 39.7 GHz, Chebyshev response with 0.1-dB ripple; and
Skirt selectivity	−20 dB at 500 MHz away from passband edge.

The measured results in Fig. 8 show about 2-dB insertion loss in the passband and about 200-MHz downward shift for the center frequency.

In the experiments performed, the measured center frequencies are always lower than the calculated values. The deviations range from 170 MHz to 300 MHz. One cause of this shift is due to the way the filter is assembled. To support the substrate in the waveguide, 10-mil-deep grooves are machined into the top and bottom walls. An experimental study on this effect shows that within the quarter-wavelength range, the deeper the groove is made, the more the center frequency will shift down. In addition, another possible source of the discrepancy is the finite thickness of the metal fin. The thickness effect is minor at this frequency since the thickness of the copper cladding on the substrate is about 0.5 mil. However, it will become an important factor for higher frequency applications, such as *W*-band circuits. These effects are currently under study.

From the experiments, it has been observed that the insertion loss of a unilateral fin-line filter is always greater than that of a bilateral filter for similar design specifications. One possible explanation is that the dielectric loss of the unilateral filter is greater, while the conductor loss is about the same in both cases. In the case of bilateral fin-lines, little energy can penetrate into the very narrow space between the strips. Therefore, the energy is mainly

coupled through the wider empty waveguide section. In the unilateral case, the energy is coupled about evenly through the empty guide and the partially dielectric-filled guide region. Obviously, more dielectric loss is encountered in this case. By the same reasoning we can surmise that the conductor loss is about the same for both cases. Although the bilateral structure has copper cladding on both sides of the substrate, there is essentially no current flowing on the inner surface facing the dielectric. It is thus equivalent to a conducting strip with current flowing on the outer surface of both sides as in the unilateral case. Of course, these statements are strictly conjectural; further study is needed to verify them. This conjecture would also be applicable to the case of insulated fin-lines versus bilateral fin-lines.

Another point worth mentioning is the sensitivity of the filter structure to mechanical tolerances. Calculations show that for both cases, the center frequency shifts about 100 MHz if the fabrication error in resonator length is 1 mil. Also, if the dielectric substrate is shifted in the broadwall direction (x-direction) from its centered position, the filter's center frequency falls. This effect is much more noticeable with the unilateral structure. Therefore, the bilateral structure shows more promise from a constructional viewpoint.

V. Conclusions

We presented an efficient CAD algorithm based on an exact analysis for a class of E-plane bandpass filters. Filters for Ka-band applications have been fabricated based on the present design. Measured characteristics agree well with theoretical data. Extensive experiments show that the bilateral construction is more promising than the unilateral structure.

Appendix I
Expressions for H_n, F_n, and G_n

The coefficients H_n, F_n, and G_n are related to the structure geometry and the field distribution in Regions I, II, and III, respectively. They are derived from the overlapping integrals

$$\int_0^b \phi_m^{\mathrm{I}}(x)\phi_n^{\mathrm{II}}(x)\,dx = \frac{H_m F_n}{\gamma_n''^2 - \gamma_m'^2} \tag{A1}$$

$$\int_b^a \phi_m^{\mathrm{I}}(x)\phi_n^{\mathrm{III}}(x)\,dx = \frac{H_m G_n}{\gamma_n'''^2 - \gamma_m'^2} \tag{A2}$$

where $\phi_i^{\mathrm{I}}(x)$, $\phi_i^{\mathrm{II}}(x)$, and $\phi_i^{\mathrm{III}}(x)$ are the ith order orthonormal eigenfunctions for the E_y fields in Regions I, II, and III, respectively (refer to Fig. 2). The expressions for H_i, F_i, and G_i of different geometries are given in the following.

Metallic E-Plane Structure

$$H_n = \sqrt{\frac{2}{a}}\sin\frac{n\pi b}{a} \tag{A3a}$$

$$F_n = (-1)^n\sqrt{\frac{2}{b}}\,\frac{n\pi}{b} \tag{A3b}$$

$$G_n = (-1)^n\sqrt{\frac{2}{c}}\,\frac{n\pi}{c}. \tag{A3c}$$

Bilateral Fin-Line Structures

$$H_n = A_n\cos\xi_n b \tag{A4a}$$

$$F_n = (-1)^n\sqrt{\frac{2}{b}}\,\frac{\left(n-\frac{1}{2}\right)\pi}{b} \tag{A4b}$$

$$G_n = (-1)^n\sqrt{\frac{2}{c}}\,\frac{n\pi}{c} \tag{A4c}$$

where

$$A_n = \sqrt{2}\left[b + \frac{\sin\xi_n b\cos\xi_n b}{\xi_n} + \left(c - \frac{\sin\eta_n c\cos\eta_n c}{\eta_n}\right)\left(\frac{\cos\xi_n b}{\sin\eta_n c}\right)^2\right]^{-1/2}$$

and where ξ_n and η_n are x-components of nth order wavenumber in the dielectric and the air region, respectively.

Unilateral Fin-Line Structures

$$H_n = A_n C_n \sin\eta_n c \tag{A5a}$$

$$F_n = -B_n\xi_n'\frac{\sin\eta_n' e_1}{\sin\xi_n' e_2} \tag{A5b}$$

$$G_n = (-1)^n\sqrt{\frac{2}{c}}\cdot\frac{n\pi}{c} \tag{A5c}$$

where

$$A_n = \sqrt{2}\left[d - \frac{\sin\eta_n e_1\cos\eta_n e_1}{\eta_n} + \eta_n^2 e_2\left(\frac{\sin^2\eta_n e_1}{\eta_n^2} + \frac{\cos^2\eta_n e_1}{\xi_n^2}\right) + C_n^2\left(c - \frac{\sin\eta_n c\cos\eta_n c}{\eta_n}\right) + C_n\frac{\eta_n^2\sin\xi_n e_2}{\xi_n}\cdot\left(\frac{\sin\eta_n e_1\sin\eta_n c}{\eta_n^2} + \frac{\cos\eta_n e_1\cos\eta_n c}{\xi_n^2}\right)\right]^{-1/2}$$

$$C_n = \frac{\eta_n}{\sin\eta_n c}\left(\frac{\sin\eta_n e_1\cos\xi_n e_2}{\eta_n} + \frac{\sin\xi_n e_2\cos\eta_n e_1}{\xi_n}\right)$$

$$B_n = \sqrt{2}\left[e_1 - \frac{\sin\eta_n' e_1\cos\eta_n' e_1}{\eta_n'} + \left(e_2 - \frac{\sin\xi_n' e_2\cos\xi_n' e_2}{\xi_n'}\right)\left(\frac{\sin\eta_n' e_1}{\sin\xi_n' e_2}\right)^2\right]^{-1/2}$$

and where $\xi_n(\xi_n')$ and $\eta_n(\eta_n')$ are the nth order wavenumber of dielectric (air) part in Regions I and II, respectively.

Appendix II
Equivalent Circuit of a Strip

The equivalent T network for a finite-length septum is shown in Fig. 9. The values of the normalized reactance x_s and x_p are to be calculated from the scattering parameters

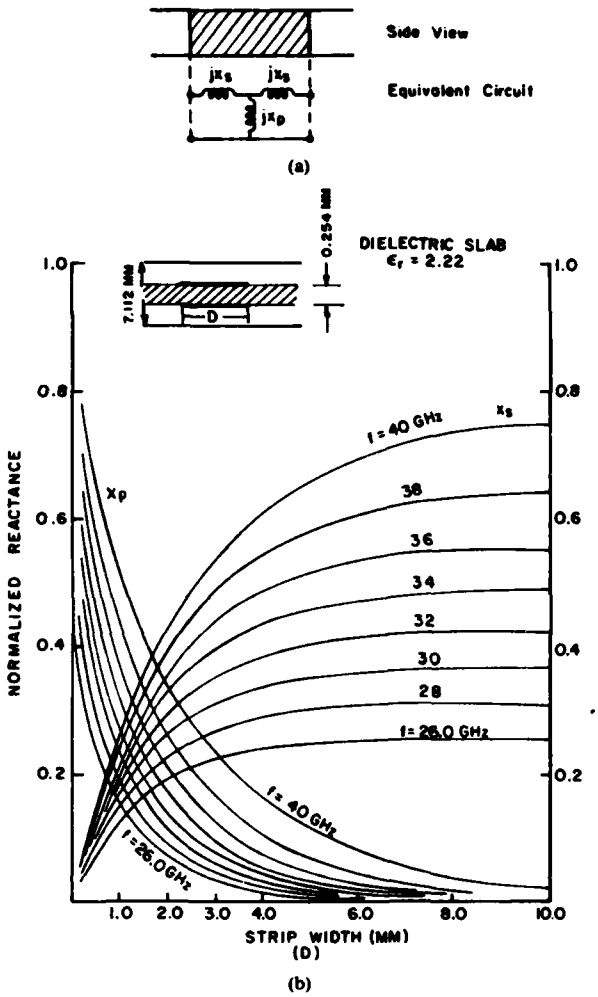

Fig. 9. Equivalent circuit for a finite-length septum. (a) Equivalent circuit. (b) Plot of reactances x_s and x_p versus septum length.

of a septum of length, say, w. Let the scattering matrix of the fundamental mode be

$$S = \begin{bmatrix} S_{11} & S_{12} \\ S_{21} & S_{22} \end{bmatrix}. \tag{A6}$$

For this reciprocal lossless two-port device, the following relations hold:

$$S_{12} = S_{21} \tag{A7}$$

$$S_{11} = S_{22} \tag{A8}$$

$$|S_{11}|^2 + |S_{22}|^2 = 1. \tag{A9}$$

These relations provide useful error-checking criteria for the numerical calculation.

If we convert the scattering matrix into impedance matrix and equate it to the impedance matrix of the equivalent T network, we have

$$[\bar{Z}] = [I+S][I-S]^{-1} = \begin{bmatrix} jx_s + jx_p & jx_p \\ jx_p & jx_s + jx_p \end{bmatrix} \tag{A10}$$

where I is the identity matrix. By equating the elements in the matrix on both sides, x_s and x_p are uniquely determined

$$jx_p = \frac{2S_{12}}{(1-S_{11})^2 - S_{12}^2} \tag{A11}$$

$$jx_s = \frac{1 - S_{12} + S_{11}}{1 - S_{11} + S_{12}}. \tag{A12}$$

Fig. 9 shows the calculated values for x_s and x_p as a function of septum length w with frequency as parameters.

References

[1] Y. Konishi and K. Uenakada, "The design of a bandpass filter with inductive strip-planar circuit mounted in waveguide," *IEEE Trans. Microwave Theory Tech.*, vol. MTT-22, pp. 869–873, Oct. 1974.

[2] Y. Tajima and Y. Sawayama, "Design and analysis of a waveguide-sandwich microwave filter," *IEEE Trans. Microwave Theory Tech.*, vol. MTT-22, pp. 839–841, Sept. 1974.

[3] P. J. Meier, "Integrated fin-line millimeter components," *IEEE Trans. Microwave Theory Tech.*, vol. MTT-22, pp. 1209–1216, Dec. 1974.

[4] A. M. K. Saad and K. Schünemann, "Design and performance of fin-line bandpass filters," *9th Eur. Microwave Conf.*, (Brighton, England), Sept. 17–20, 1979.

[5] F. Arndt *et al.*, "Low-insertion-loss fin-line filters for millimeter-wave applications," *11th Eur. Microwave Conf.* (Amsterdam, Netherlands), Sept. 7–10, 1981, pp. 309–314.

[6] R. Mittra and S. W. Lee, *Analytical Techniques in the Theory of Guided Waves*. New York: Macmillan, 1971, pp. 45–54.

[7] C. F. Vanblaricum, Jr. and R. Mittra, "A modified residue-calculus technique for solving a class of boundary value problems—Part II: Waveguide phased arrays, modulated surfaces, and diffraction gratings," *IEEE Trans. Microwave Theory Tech.*, vol. MTT-17, pp. 310–319, June 1969.

[8] T. E. Rozzi and W. F. G. Mecklenbräuker, "Wide-band network modeling of interacting inductive irises and steps," *IEEE Trans. Microwave Theory Tech.*, vol. MTT-23, pp. 235–245, Feb. 1975.

[9] Routin ZXMIN, IMSL Library 3 (for CDC Cyber 70/6000/7000 series). See IMSL Library Manual.

[10] J. W. Bandler, "Optimization method for computer-aided design," *IEEE Trans. Microwave Theory Tech.*, vol. MTT-17, pp. 533–562, Aug. 1969.

[11] P. J. Meier, "Equivalent relative permittivity and unloaded Q factor of integrated fin-line," *Electron. Lett.*, vol. 9, no. 7, pp. 162–163, Apr. 1973.

Yi-Chi Shih (SM'80) was born in Taiwan, the Republic of China, on February 8, 1955. He received the B. Eng. degree from National Taiwan University, Taiwan, R.O.C., in 1976, and the M.Sc. degree from the University of Ottawa, Ontario, Canada, in 1980, both in electrical engineering. Since 1980 he has been working toward the Ph.D. degree at The University of Texas at Austin.

His research interest includes the analysis and design of microwave and millimeter-wave components.

Tatsuo Itoh (SM'74–F'82) received the Ph.D. degree in electrical engineering from the University of Illinois, Urbana, in 1969. From September 1966 to April 1976 he was with the Electrical Engineering Department, University of Illinois. From April 1976 to August 1977 he was a Senior Research Engineer in the Radio Physics Laboratory, SRI International, Menlo Park, CA. From August 1977 to June 1978 he was an Associate Professor at the University of Kentucky, Lexington. In July 1978, he

joined the faculty at the University of Texas at Austin, where he is now a Professor of Electrical Engineering and Director of the Microwave Laboratory. During the summer 1979 he was a Guest Researcher at AEG-Telefunken, Ulm, West Germany.

Dr. Itoh is a member of the Institute of Electronics and Communication Engineers of Japan, Sigma Si, and Commission B of USNC/URSI. He serves on the Administrative Committee of IEEE Microwave Theory and Techniques Society. He is a Professional Engineer registered in the State of Texas.

Long Q. Bui was born in Hue, South Vietnam, on May 6, 1952. He received the B.S. Degree in electrical engineering in 1976, and the M.S.E.E. degree in 1981, both from the University of Texas at Austin, TX.

He has been with Hughes Aircraft Company, Torrance, CA, since 1979 as a Member of Technical Staff on Advanced Component Developments for millimeter-wave applications. His main research interests are concerned with planar circuit techniques for mixers, filters, multiplier designs, and computeraided techniques for design and manufacture.

APPENDIX 3

Field analysis of Millimeter-wave GaAs Double-drift IMPATT Diode in the Travelling-wave Mode *

Yoshiro Fukuoka and Tatsuo Itoh

Department of Electrical Engineering
University of Texas at Austin
Austin, Texas 78712

Abstract

An analysis of a realistic model of distributed IMPATT structures is described. Wave equations are solved with all losses included. The results show that net gain is produced at frequencies just above the avalanche resonance, while the propagation becomes slow at high frequencies. The results compare favorably with experiment.

---

* This work was supported in part by the Joint Service Electronics Program under Grant F49620-82-0033 and in part by the U.S. Army Research Office under Contract DAAG29-81-K-0053.

Field analysis of Millimeter-wave GaAs Double-drift IMPATT Diode in the Travelling-wave Mode *

Yoshiro Fukuoka and Tatsuo Itoh

Department of Electrical Engineering
University of Texas at Austin
Austin, Texas 78712

Abstract

An analysis of a realistic model of distributed IMPATT structures is described. Wave equations are solved with all losses included. The results show that net gain is produced at frequencies just above the avalanche resonance, while the propagation becomes slow at high frequencies. The results compare favorably with experiment.

---

* This work was supported by the Office of Naval Research, contract N00014-79-0053, Joint Service Electronics Program F49620-82-0033, and US Army Research Office contract DAAG29-81-K-0053.

Introduction

An IMPATT diode is an attractive source at millimeter-wave frequencies because of its feasibility of producing a large power. However, as frequencies become higher, it tends to be difficult to use sufficient device area mainly because thinner depletion layer is required for IMPATT operation. A travelling-wave structure is one way of efficiently utilizing larger area of the device [1-3]. The electromagnetic wave travelling along pn junction draws some energy out of dc current and is therefore amplified.

The most elaborate theoretical treatment of such a structure so far was done by Franz et.al. [4]. However, their model was still too simplified because inactive layers were all assumed to be perfect conductors and the avalanche region in the depletion layer was assumed to be infinitesimally thin. At mm-wave frequencies, however, the effect of the finite conductivities of these inactive regions is important. They contribute to loss and affect phase constants of the device.

In the present work, a complete set of differential equations governing both wave propagation and avalanche multiplication is solved with boundary conditions including the finite conductivities of the metal contacts. Small-signal assumption is made, and results are presented for a GaAs double-drift IMPATT diode. Computed gain and propagation constants are compared with experimental results published by other authors. They are qualitatively in agreement.

Theory

The structure to be studied is a one dimensional multilayered waveguide (Fig.1), where materials change only in the x direction. In the figure,

if a single-drift diode is considered, two center regions (n and p) should be replaced with a single material. Also, it should be noted that the metal contact is usually made of a couple of different conductors. In such a structure the dominant propagating mode is a TM mode, which has only the y component of magnetic field and the x and z components of electric field. The expressions of these components in the inactive regions are obtained in a usual way.

In the IMPATT medium, the governing differential equations are as follows [4,5]:

$$\nabla^2\vec{E} - \nabla(\nabla\cdot\vec{E}) - \mu\varepsilon\frac{\partial^2\vec{E}}{\partial t^2} - \mu\frac{\partial\vec{J}_c}{\partial t} = 0$$

$$\nabla\cdot\vec{E} = \frac{q}{\varepsilon}\left(N_D - N_A + p - n \right)$$

$$\frac{\partial n}{\partial t} = \frac{1}{q}\left(\nabla\cdot\vec{J}_n + \alpha|J_n| + \beta|J_p| \right)$$

$$\frac{\partial p}{\partial t} = \frac{1}{q}\left(-\nabla\cdot\vec{J}_p + \alpha|J_n| + \beta|J_p| \right)$$

(1)

where

E	: electric field	J_c	: conduction current
J_n	: electron current	J_p	: hole current
N_D	: donor concentration	N_A	: acceptor concentration
n	: electron concentration	p	: hole concentration
α	: genaration rate for electrons	β	: genaration rate for holes
q	: unit charge	ε	: permittivity
μ	: permeability		

Each variable quantity is decomposed into dc and ac (or rf) parts and solved separately. For example,

$$E_x = E_{xDC} + \tilde{E}_x e^{j\omega t - \gamma z}$$

It is reasonable to consider that only x-component of dc electric field exists, therefore dc equations are solved in a similar way as presented by Misawa [6]. This also determines the thickness of the space-charge region (active region). Using the solution of dc equations, ac equations are solved with boundary conditions which require H_y and E_z to be continuous at each boundary.

Calculations in the active region are done by finite difference method, and 100 steps are usually sufficient for accurate calculations because the field functions are smooth.

Results

The parameters chosen for the numerical calculations are shown in Table 1. The structure consists of 8 layers and is very similar to the one used in the experiment made by Bayraktaroglu et.al. [7].

The computed results for gain and propagation constants are presented in Fig. 2 and 3, respectively. As frequency becomes lower and approaches to the avalanche resonance, gain increases and the wave propagation becomes faster. In these figures, dotted lines indicate the results for the special case that the depletion region is replaced by a lossless material. Propagation becomes slow wave in this case. Each curve asymptotically approaches to the dotted line at high frequencies, since the device deviates from the IMPATT operation.

Fig. 4 shows the comparison of the present theory and the experimental results obtained in [7]. The device was used as an oscillator with one end open and the other short. In the figure, white dots (o) show the actual device lengths and the oscillation frequency obtained in the experiment, and black dots (•) show one-third of the actual device length (i.e., they are considered to be oscillating at three-quarter wavelength). Three solid curves indicate the theoretical quarter wavelength where net gain is produced in the device. They are in good agreement except two black dots where higher order resonance ($3\lambda/4$) takes place and the actual terminating condition might be more prominent to affect the oscillation frequencies.

Finally, Fig. 5 shows how gain changes with respect to the dc current. As the dc current increases, the gain also increases but suddenly goes to a large loss at certain point. This fact qualitatively agrees with the results of power measurements for the conventional IMPATT diodes [8].

Conclusion

Wave propagation phenomena in the travelling-wave IMPATT diode were analyzed numerically, and reasonable results were obtained. It was shown that the propagation was slow wave at high frequencies, but became fast as approaching to the avalanche resonance of the IMPATT medium. The mechanism of producing the fast wave is not yet clear, and investigation is currently being made.

References

1. T. A. Midford and H. C. Bowers, "A Two-Port IMPATT Diode Travelling Wave Amplifier," Proc. IEEE, pp.1724-1725, Oct., 1968.

2. N. S. Davydova, Yu. Z. Danyushevskiy and L. I. Telyatnikov, "Linear Theory of an IMPATT Diode Distributed Microwave Amplifier," Telecommun. Radio Eng., vol.27, no.8, pp.112-115, Aug., 1972.

3. K. G. Hambleton and P. N. Robson, "Design Consideration for Resonant Travelling Wave IMPATT Oscillators," Int. J. Electronics, vol.35, no.2, pp.225-244, 1973.

4. M. Franz and J. B. Beyer, "The Travelling-Wave IMPATT Mode," IEEE Trans. Microwave Theory Tech., vol.MTT-25, no.11, pp.861-865, Nov., 1978.

5. D. L. Scharfetter and H. K. Gummel, "Large-Signal Analysis of a Silicon Read Diode Oscillator," IEEE Trans. Electron Devices, vol.ED-16, no.1, pp.64-77, Jan., 1969.

6. T. Misawa, "Negative Resistance in p-n Junctions Under Avalanche Breakdown Conditions, Part II," IEEE Trans. Electron Devices, vol.ED-13, no.1, pp.143-151, Jan., 1966.

7. B. Bayraktaroglu and H. D. Shih, "Millimeter-Wave GaAs Distributed IMPATT Diodes," IEEE Electron Devices Lett., vol.EDL-4, no.11, pp.393-395, Nov., 1983.

8. B. Bayraktaroglu and H. D. Shih, "Integral Packaging for Millimeter-Wave GaAs IMPATT Diodes Prepared by Molecular Beam Epitaxy," Electron. Lett., vol.19, no.9, pp.327-328, Apr., 1983.

List of figures

Fig. 1 travelling-wave double-drift IMPATT diode

Table 1 parameters used in numerical calculations

Fig. 2 gain versus frequency : Curves are shown for 3 different DC current densities.

----- : Active region is replaced by a lossless material.

-·-·- : $\sqrt{\varepsilon_r}\, k_o$

Fig. 3 propagation constant versus frequency

----- : Active region is replaced by a lossless material.

-·-·- : $\sqrt{\varepsilon_r}\, k_o$

Fig. 4 oscillation frequency versus length of device : 3 solid curves show theoretical results where net gain is positive.

o : experiment ($\lambda/4$) [7]

• : experiment ($3\lambda/4$)

----- : Active region is replaced by a lossless material.

-·-·- : $\sqrt{\varepsilon_r}\, k_o$

Fig. 5 gain versus DC current

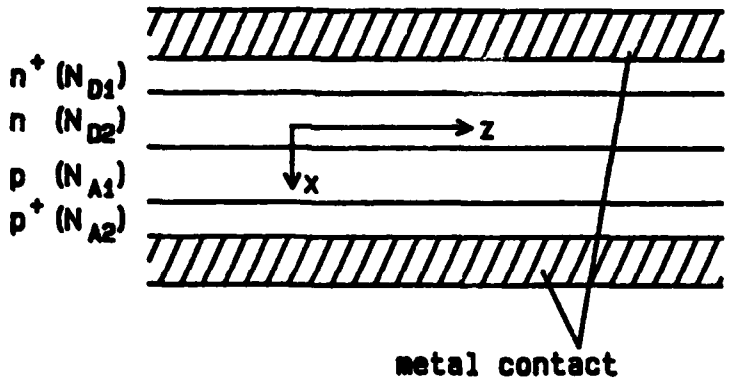

Figure 1

material	thickness	doping level	conductivity
Au	7.0 microns	—	4.3×10^{7} S/m
Ti	0.1	—	1.8×10^{6}
n^{+}-GaAs	0.2	$5.0 \times 10^{18}/cm^{3}$	6.81×10^{5}
n-GaAs	0.3	1.5×10^{17}	(2.04×10^{4})
p-GaAs	0.3	1.5×10^{17}	(9.61×10^{2})
p^{+}-GaAs	0.2	5.0×10^{18}	3.20×10^{4}
Ti	0.1	—	1.8×10^{6}
Au	7.0	—	4.3×10^{7}

TABLE 1

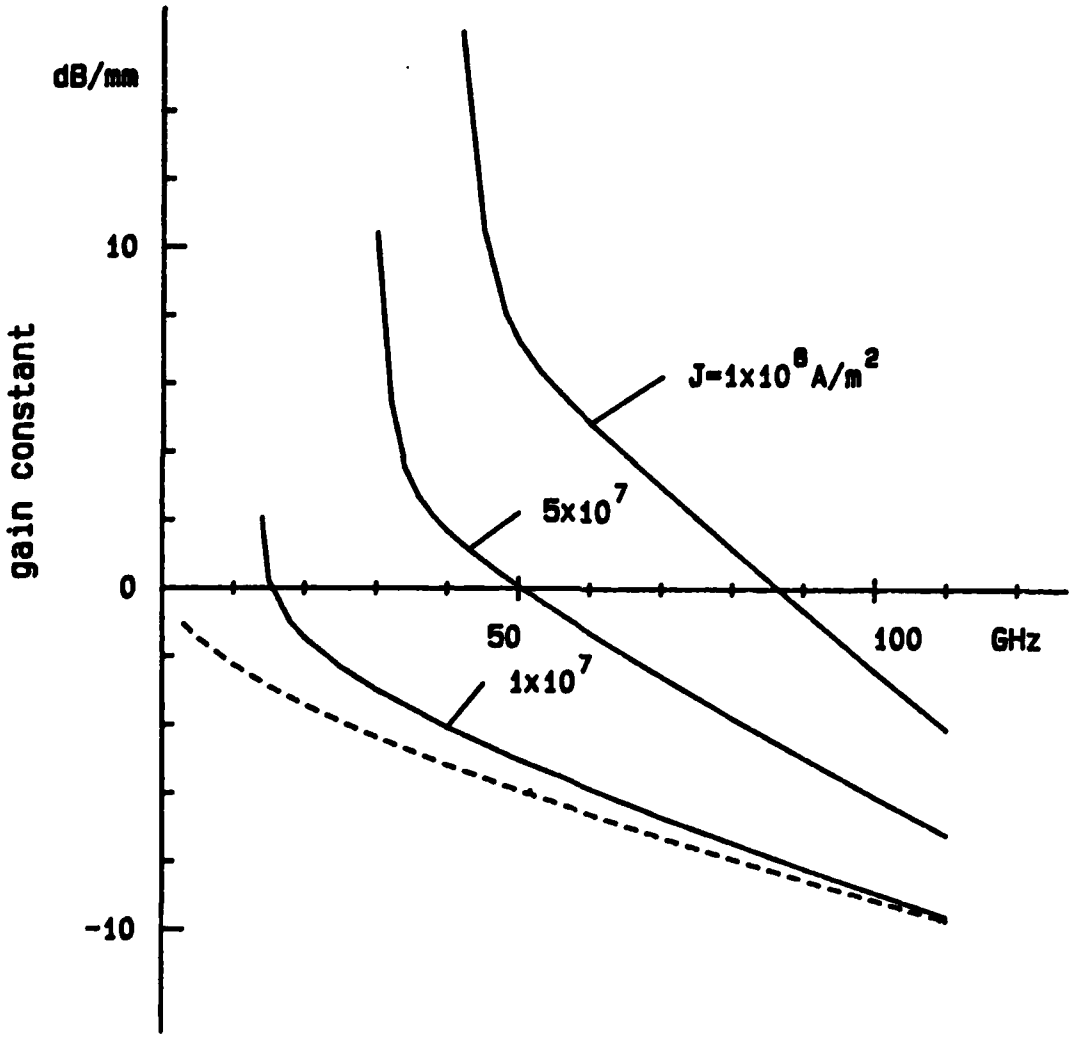

Figure 2

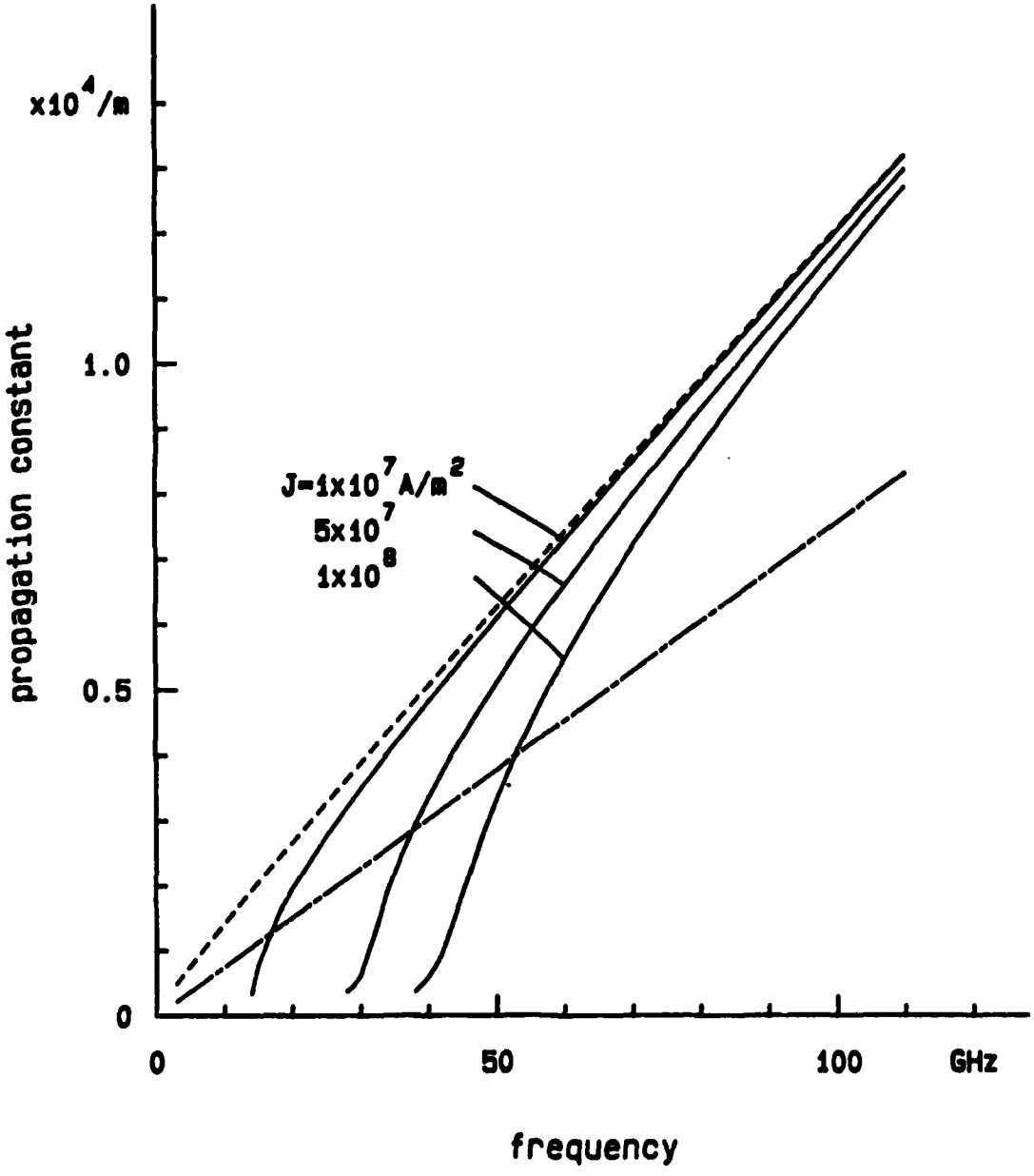
x10^4/m
propagation constant
1.0
0.5
0
J=1x10^7 A/m^2
5x10^7
1x10^8
0
50
100
GHz
frequency

Figure 3

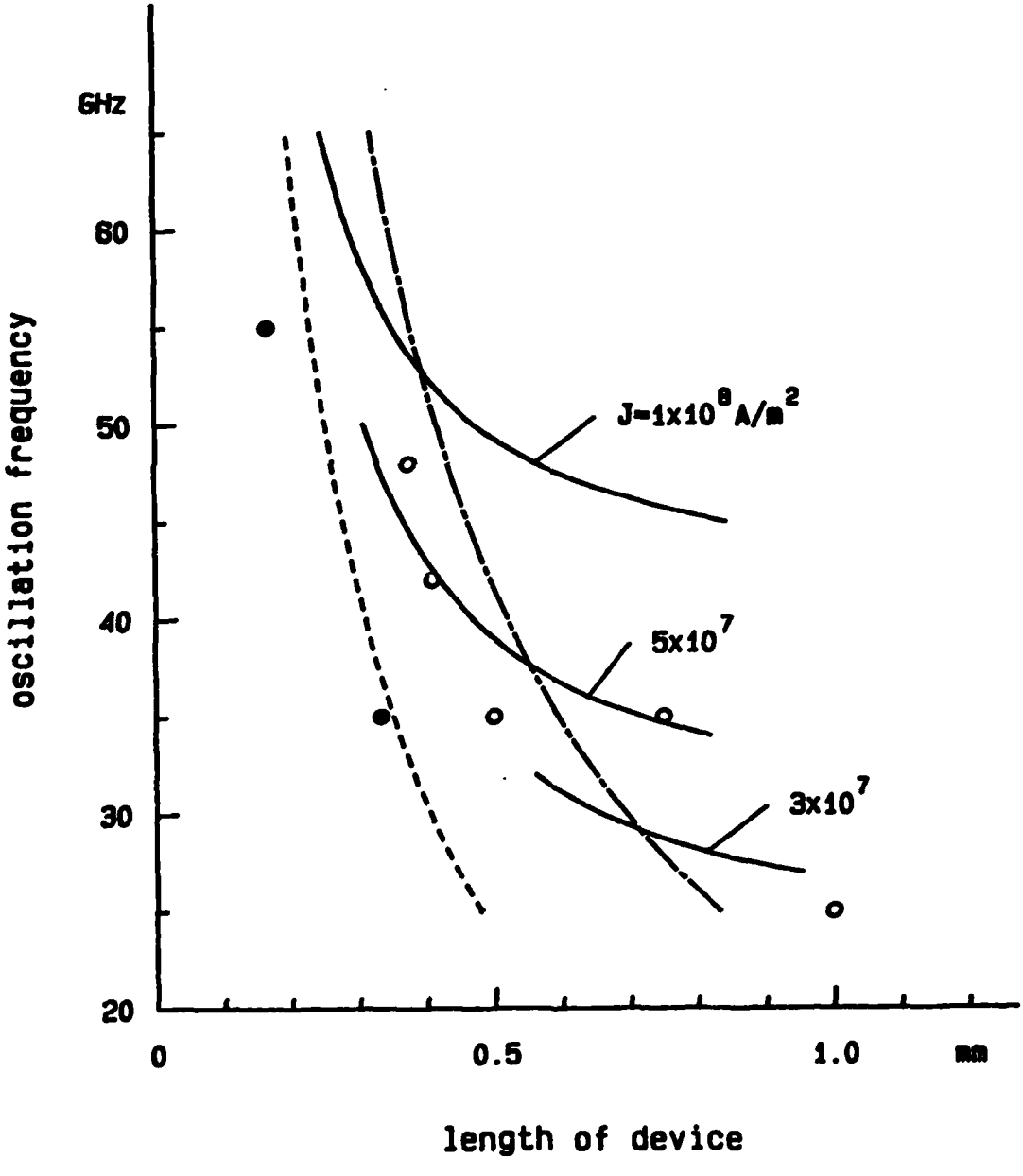
GHz
60
50
40
30
20
oscillation frequency
J=1x10^8 A/m^2
5x10^7
3x10^7
0
0.5
1.0
mm
length of device

Figure 4

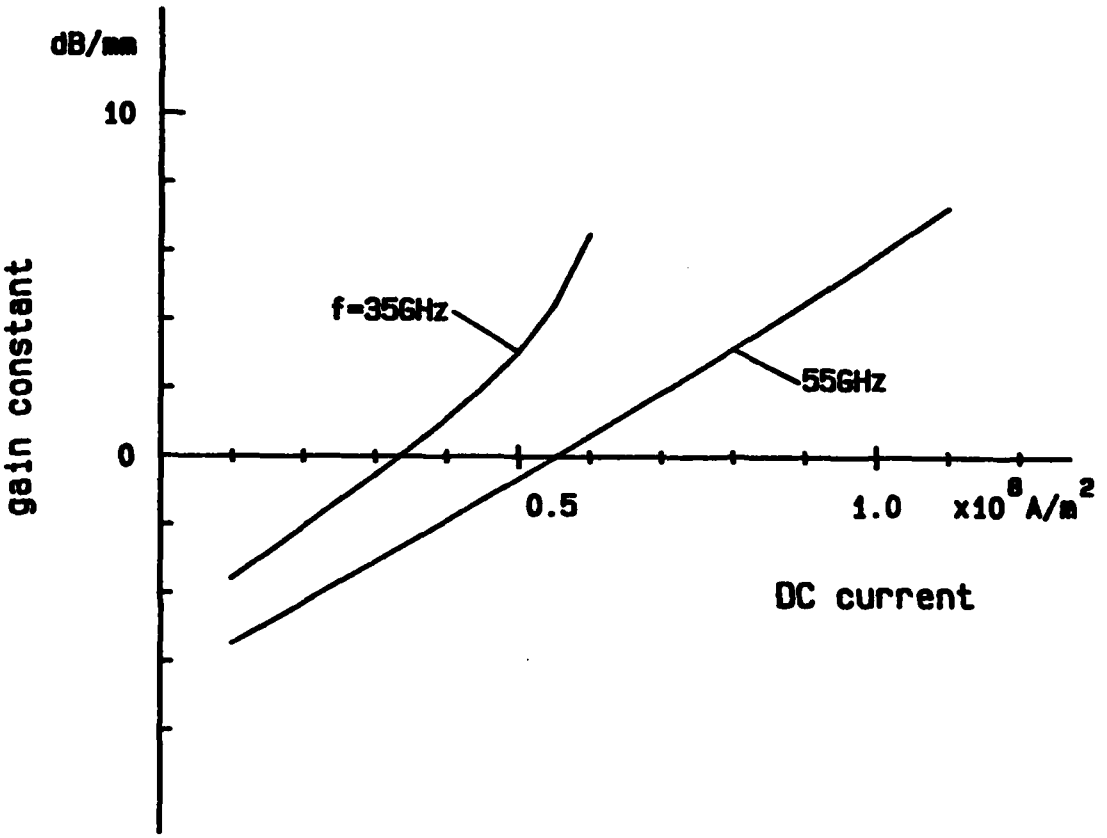
dB/mm
10
0
gain constant
f=35GHz
55GHz
0.5
1.0
x10^8 A/m^2
DC current

Figure 5

APPENDIX 4

International Journal of Infrared and Millimeter Waves, Vol. 5, No. 6, 1984

COPLANAR SCHOTTKY VARIABLE PHASE SHIFTER CONSTRUCTED ON GaAs SUBSTRATE FOR MILLIMETER-WAVE APPLICATION*

Yoshiro Fukuoka and Tatsuo Itoh

Department of Electrical Engineering
University of Texas at Austin
Austin, Texas 78712

Received February 8, 1984

A Schottky contact variable phase shifter constructed on either uniformly or periodically doped GaAs substrate is discussed in details. The device can operate at millimeter-wave frequencies with reasonably low attenuation.

Key words: phase shifter, coplanar waveguide, slow wave, millimeter-wave integrated circuit

Introduction

A millimeter-wave integrated circuits has drawn more interests because of its compact size and reliability, and studies have been done for various device components. In order to realize this kind of integration, it is essential to have accurate means to design each device component. Also, it is preferrable that the device has a simple structure.

A metal-insulator-semiconductor (MIS) coplanar waveguide has recently studied as it has a slow-wave characteristic (1-3). The rate of slow-wave propagation depends on the thickness of the insulator region. Therefore if the

* Work supported by the Office of Naval Research under Contract N00014-79-0053, Joint Service Electronics Program under Grant F49620-82-C-0033, and US Army Research Office under Contract DAAG29-81-K-0053.

0195-9271/84/0600-0793$03.50/0

Schottky contact is used in this structure, the phase shift in the device can be electronically controlled (4). This structure is suitable for integration because of its simple form, and also, the coplanar configuration makes it easy to connect other circuit components both in series and parallel. However, various studies so far show that these devices have increasing attenuation as the operating frequency becomes higher, which makes the application of such a device at mm-wave frequencies difficult. To reduce such attenuation, we recently introduced a periodic structure where undoped substrate sections are inserted periodically (5). This structure has an advantage of reducing the loss as well as extending the range of slow-wave propagation at high frequencies.

The present paper discusses the optimum conditions for both uniform and periodic Schottky contact coplanar waveguides as variable phase shifters. Under such conditions, it is possible to achieve 180° phase shift at mm-wave frequencies without significant attenuation.

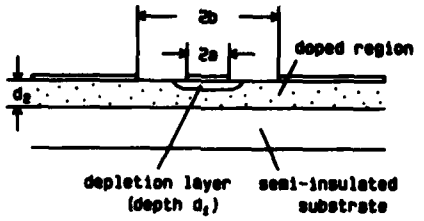

a

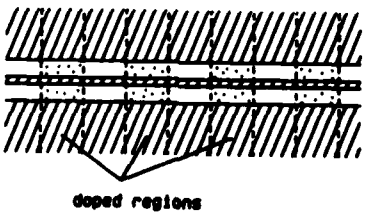

b

Figure 1. Schottky coplanar waveguide
a Cross-sectional view
b Top view of Schottky periodic coplanar waveguide

Theoretical Calculation

The structure under discussion is shown in Fig.1. Fig.1a shows the cross section of the Schottky coplanar waveguide. To analyze this structure, an efficient point-matching method is introduced (5). In order to utilize this method, the depletion layer of the Schottky contact needs to be modeled by a lossless layer with the same constant thickness extending in the horizontal direction. The relation between the DC bias voltage and the thickness of the depletion layer can be calculated by the well known equation (4). Since the depth of the depletion layer is small and the field is confined under the center conductor, the error introduced by this model is considered to be negligible. Typically, 25 matching points and 500 basis functions were used for most calculations in this paper. It takes about 20 seconds for the calculation of both propagation constant and characteristic impedance. Fig.1b shows the top view of the periodic structure. In order to analyze this structure, this point-matching method is used twice for both doped and undoped sections to obtain propagation constants and characteristic impedances, and then Floquet's theorem is used to calculate the overall characteristic of the periodic structure. The method was proven to be accurate and justified by experiment (5).

Optimum Operation

The important parameters to be considered for an optimum operation condition, are the dimensions of the coplanar waveguide, the conductivity and the thickness of the doped region, and the depletion layer thickness. It is known that, at a fixed frequency, there is a certain value of the conductivity of the doped region that yields a maximum range of slow-wave frequency region (3). This conductivity also gives a minimum attenuation over the certain range of conductivity. Therefore it is first important to choose an impurity concentration of the doped region so that the conductivity becomes this optimum value. However, the impurity level is limited to a certain value, because the breakdown voltage becomes low when the impurity concentration is large. For this reason, a useful value of the conductivity of the doped region in GaAs substrate is limited up to 10^4 to 10^5 S/m.

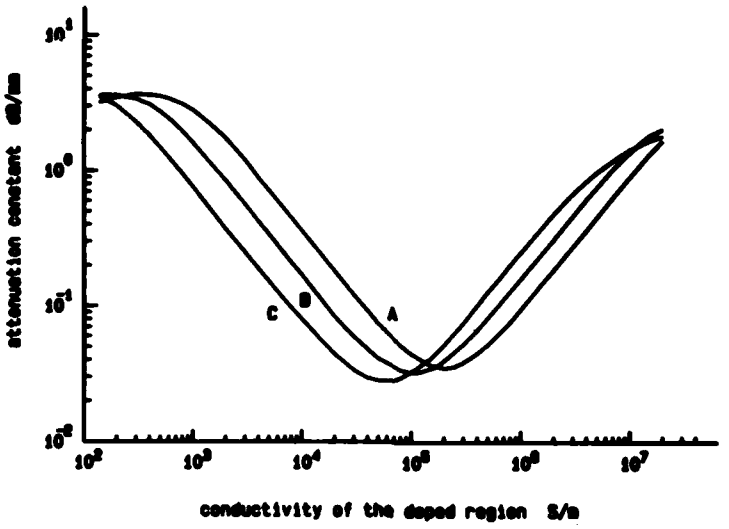

Figure 2. Behavior of the optimum conductivity with respect to the thickness of the doped region
curve A ... d_2 = 0.5 microns
B ... 1.0
C ... 10.0

Fig.2 shows the behavior of this optimum conductivity at 10 GHz. Three curves are drawn to show the effect of the thickness of the doped region d_2. It is interesting that increased value of d_2 shifts the point of minimum attenuation to the left, i.e. the optimum conductivity is lowered. Also the minimum value of the attenuation constant is slightly lowered. Therefore it is necessary to set d_2 to a proper value. This tendency, however, disappears when d_2 exceeds a certain value, e.g. 10 microns in this case. The attenuation constant also depends on width of both the center conductor and the slot. Fig.3 shows this dependence. The relation is simple: the narrower the widths, the lower the attenuation. However our calculation does not include the effect of conductor loss, and it is expected that having a very narrow center conductor causes large attenuation. Also there is a limit on the slot width because the breakdown voltage of the semiconductor substrate is low.

There is one more parameter to consider: depletion

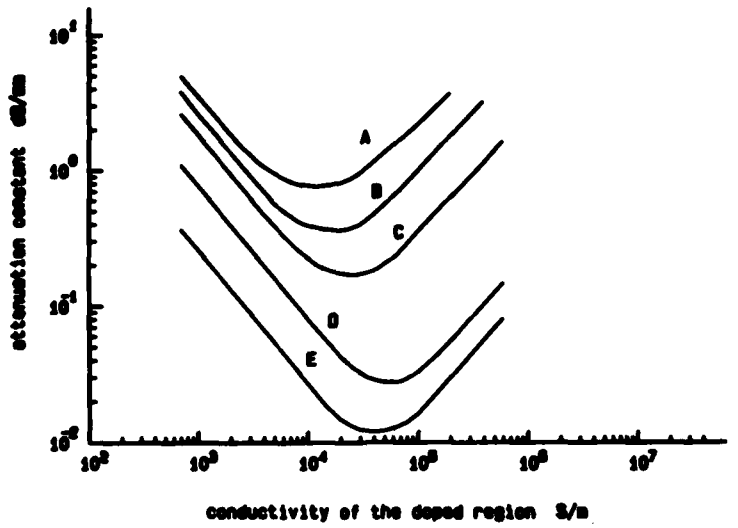

Figure 3. Dependence of the attenuation constant on the widths of the center conductor and slot (d_1 = 0.1 micron, d_2 = 10 microns, 10 GHz)
curve A ... a = 1.0 micron, b = 20.0 microns
B ... 1.0 , 10.0
C ... 1.0 , 5.0
D ... 1.0 , 1.5
E ... 0.25 , 1.5

layer thickness d_1. The thickness d_1 is determined by the DC bias voltage, and as we discussed earlier, it changes the phase shift of the device. However, it also changes the attenuation constant. This is inherent to this structure, but it is desirable to keep this change as small as possible. Fig.4 is drawn for 2 different values of d_1. The figure shows that the small values of d_1 yields large attenuation. Also, the point of minimum attenuation moves as d_1 changes. This means that we would like to use point A rather than B to keep the total change in attenuation small.

Results

According to the above discussion, we can now construct a model for the optimum operation of the Schottky

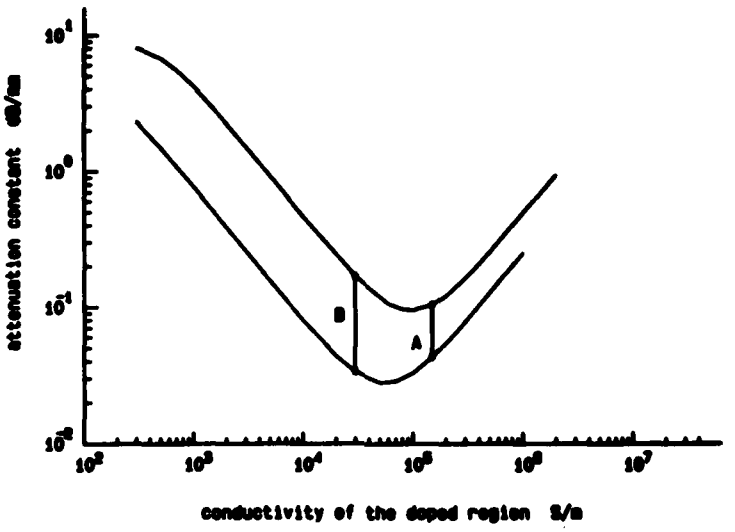

Figure 4. Dependence of the attenuation constant on the depletion layer thickness
(a = 1.0 micron, b = 1.5 microns, d_2 = 10.0 microns, 10 GHz)
upper curve ... d_1 = 0.02 microns
lower curve ... 0.1

variable phase shifter. Various constants for GaAs substrate used in our calculation are shown in Table I. The width of the center conductor of the coplanar waveguide is chosen to be 2 microns (a=1 micron). In this case, doping density in the doped region $N_d = 3 \times 10^{17}$ /cm^3, which yields the conductivity of 4.1×10^4 S/m, gives the lowest attenuation. This value gives a calculated maximum depletion layer thickness of $d_{1max} = 0.12$ microns when the DC bias voltage becomes $V_c = 1.9$ V, which is the maximum voltage that can be applied in this situation (breakdown voltage).

Using these values, the length of the device required for 180° phase shift and the total attenuation in the device are calculated. The depth of the depletion layer is varied from 0.03 to 0.09 microns, which corresponds to adjusting V_c from 0.2 to 1.7 V. The results are shown in Fig.5. This figure is drawn as follows; for each value of b, the total device length required for 180° phase shift is

Table I. Various constants for GaAs substrate used in the calculation

dielectric constant	13.0
mobility	8500 $cm^2/V\text{-}sec$
breakdown field intensity	4.0×10^7 V/m
impurity density (doped region)	3.0×10^{17} $/cm^3$
depth of doped region (d_2)	10 microns

calculated based on the propagation constant optained by our theoretical calculation. The total attenuation is then obtained by multiplying the attenuation constant by the device length. The curves show that when the slot width becomes narrower, the total attenuation becomes smaller in spite of the longer device length required. The figure also shows that the total attenuation is smaller for the periodic structure compared to the uniform device. However this advantage becomes less when the slot width becomes very narrow. The performance of the periodic structure could have been much better if the conductivity of the doped region were higher. We could not do this because of the low breakdown voltage of GaAs. Also,because of the same limitation, we can not meet the last condition given in the

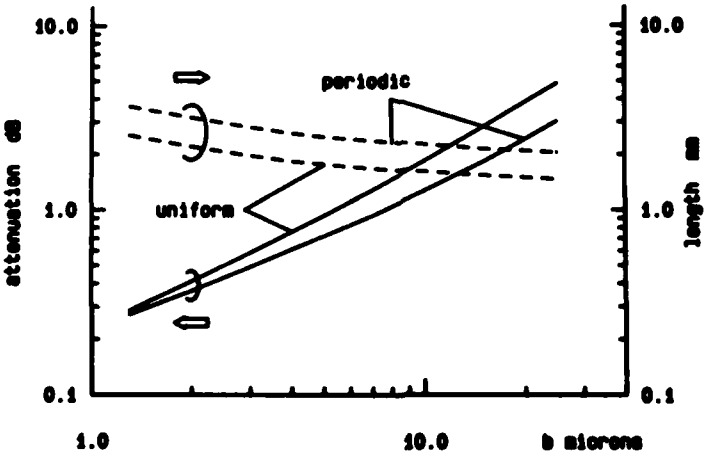

Figure 5. Required length for 180° phase shift and the total attenuation in the device

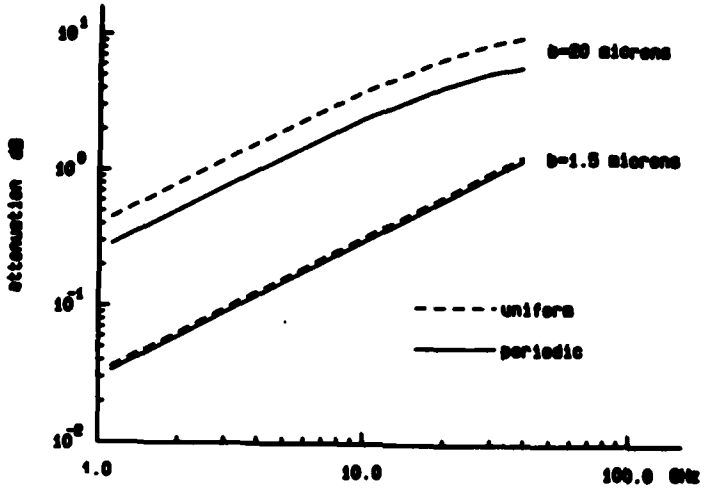

Figure 6. The total attenuation in the device at various operating frequencies

previous section: minimize the variation of the attenuation constant over the operating DC bias voltage. Therefore, if a better substrate material were used, the improvement of the performance would be possible.

Finally, the total attenuation is plotted as a function of frequency in Fig.6. For a fixed frequency, the required device length is calculated, and the total attenuation is then computed for that length. At 40 GHz and for b=1.5 microns, the calculated attenuation is 1.27 dB for the uniform device and 1.20 dB for the periodic device. Although these figures do not include conductor loss, they indicate quite satisfactory performance of these devices at mm-wave frequencies.

Conclusion

An optimum set of conditions for low loss operation of the coplanar Schottky phase shifter was discussed. Under such conditions, a model was simulated by numerical computation. Using a GaAs substrate, it was shown that these devices could be used in mm-wave frequency range, although

the advantage of using a periodic structure becomes less under these conditions.

References

1. H. Hasegawa and H. Okizaki, "M.I.S. and Schottky slow-wave coplanar striplines on GaAs substrates," Electron. Lett. 13, 663 (1977).
2. P. Kennis et al, "Properties of microstrip and coplanar lines on semi-conductor substrates," Proc. 12th Eur. Microwave Conf. 1982, pp.328-333.
3. Y.-C. Shih and T. Itoh, "Analysis of printed transmission lines for monolithic integrated circuits," Electron. Lett. 18, 585 (1982).
4. D. Jäger and W. Rabus, "Bias dependent phase delay of Schottky-contanct microstrip lines," Electron. Lett. 9, 201 (1973).
5. Y. Fukuoka and T. Itoh, "Slow-wave coplanar waveguide on periodically doped semiconductor substrate," IEEE Trans. Microwave Theory and Tech. MTT-31, 1013 (1983).

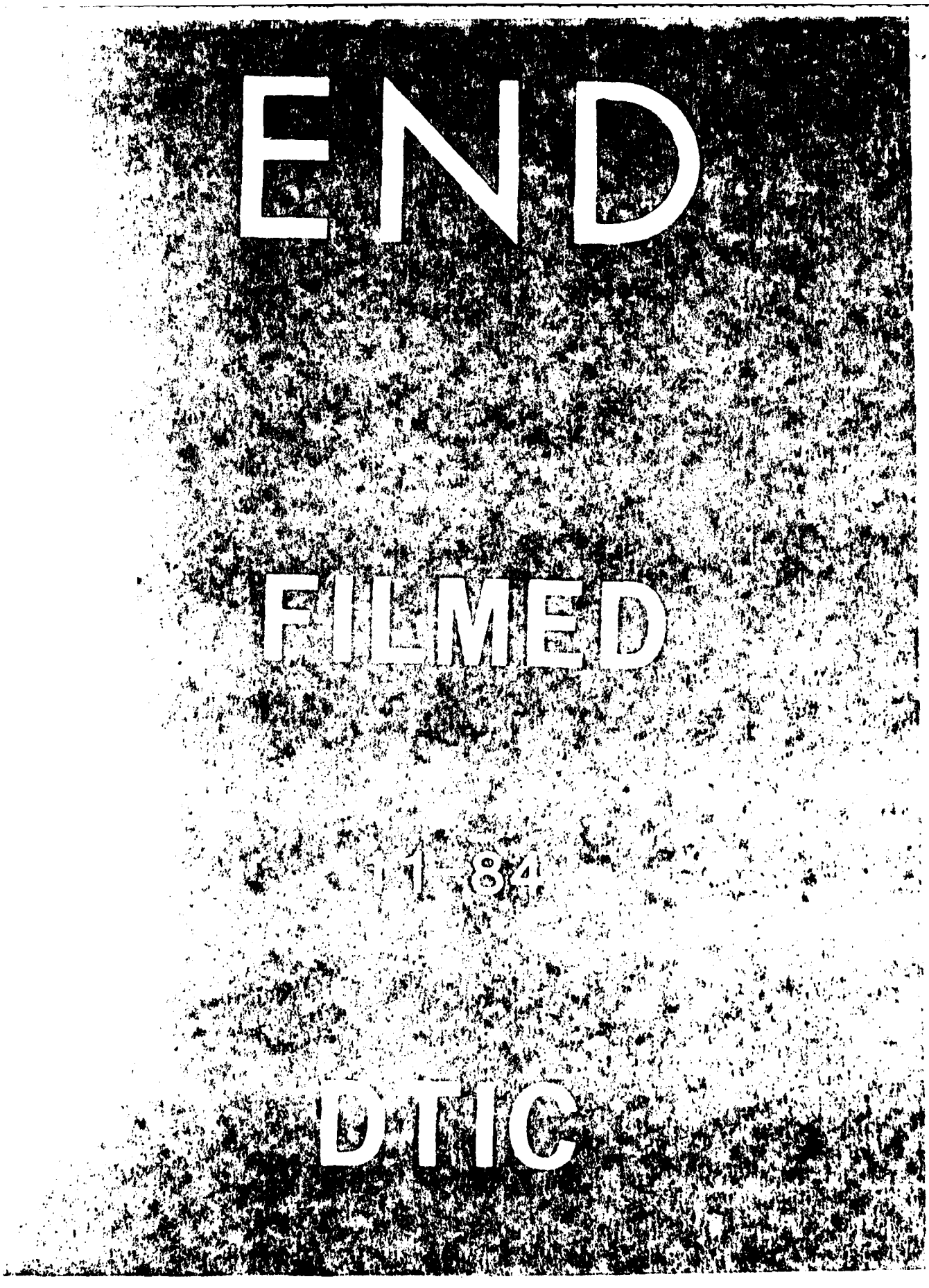
END
FILMED
1-84
DTIC